Supporting Information

Bandgap Engineering of Graphene Nanoribbons by Control over Structural Distortion

by

Yunbin Hu[1,2], Peng Xie[3] , Marzio De Corato[4,5], Alice Ruini[6,7], Shen Zhao[6], Felix Meggendorfer[3], Lasse Arnt Straasø[7], Loic Rondin[6], Patrick Simon[3], Juan Li[3,8], Jonathan J. Finley[3], Michael Ryan Hansen[9], Jean-Sébastien Lauret[6], Elisa Molinari[4,5], Xinliang Feng[10], Johannes V. Barth[3], Carlos-Andres Palma[3], Deborah Prezzi[5]*, Klaus Müllen[1]*, Akimitsu Narita[1]*

[1]Max Planck Institute for Polymer Research, Ackermannweg 10, D-55128 Mainz, Germany.
[2]Department of Organic and Polymer Chemistry, College of Chemistry and Chemical Engineering, Central South University, Changsha, Hunan 410083, P. R. China.
[3]Physik-Department, Technische Universität München, James-Franck-Str. 1, D-85748 Garching, Germany
[4]Dipartimento di Scienze Fisiche, Informatiche e Matematiche, Università di Modena e Reggio Emilia, 41125 Modena, Italy
[5]Istituto Nanoscienze, CNR, via G. Campi 213/a, 41125, Modena, Italy.
[6]Laboratoire Aimé Cotton, CNRS, Univ. Paris-Sud, ENS Cachan, Université Paris Saclay bat 505 campus d'Orsay, 91405 Orsay cedex, France.
[7]Interdisciplinary Nanoscience Center (iNANO) and Department of Chemistry, Aarhus University, Gustav Wieds Vej 14, DK-8000 Aarhus C, Denmark.
[8]Beijing Institute of Technology, 100081 Beijing, P. R. China
[9]Institute of Physical Chemistry, Westfälische Wilhelms-Universität Münster, Corrensstr. 28/30, D-48149 Münster, Germany.
[10]Center for Advancing Electronics Dresden (cfaed) & Department of Chemistry and Food Chemistry, Technische Universität Dresden, Mommsenstrasse 4, 01062 Dresden, Germany.

*Correspondence to: deborah.prezzi@nano.cnr.it,
muellen@mpip-mainz.mpg.de,
narita@mpip-mainz.mpg.de

General Methods

All reactions dealing with air- or moisture-sensitive compounds were carried out in a dry reaction vessel under argon. Preparative column chromatography was performed on silica gel from Merck with a grain size of 0.063–0.200 mm (silica gel) or 0.04–0.063 mm (flash silica gel, Geduran Si 60). Analytical thin layer chromatography (TLC) was performed on silica gel coated substrates "60 F_{254}" from Merck. Solution NMR spectra were measured on Bruker DPX 250 or AMX 300 spectrometer, and referenced to residual signals of the deuterated solvent. Abbreviations: s = singlet, d = doublet, t = triplet, m = multiplet. Matrix-assisted laser desorption/ionization time-of-flight (MALDI-TOF) mass spectra were recorded using a Bruker Reflex II utilizing a 337 nm nitrogen laser, calibrated against poly(ethylene glycol) (3,000 $gmol^{-1}$). The high-resolution electrospray ionization mass spectrometry (HR-ESI-MS) was performed on an ESI-Q-TOF system (maXis, BrukerDaltonics, Germany), where the instrument was operated in wide pass quadrupole mode for MS experiments, with the TOF data being collected between m/z 100–5000. Elemental analysis was carried out on a Foss Heraeus Vario EL as a service of the Institute for Organic Chemistry, Johannes-Gutenberg-Universität of Mainz. Analytical size exclusion chromatography (SEC) was performed on SDV PSS GPC columns using THF as eluent at a temperature of 303 K. Absorbance was determined on a UV S-3702 detector (SOMA) at a fixed wavelength of 270 nm. The samples were referenced with respect to standard polystyrene (PS) as well as poly(*p*-phenylene) (PPP) calibration curves. Solution UV–vis absorption spectra were recorded at room temperature on a Perkin-Elmer Lambda 900 spectrophotometer. The baseline was corrected by subtracting a measurement of the cuvette filled with pure solvent used for the measurement. The optical bandgap was extrapolated based on the absorption edge. GNR samples were dispersed in solvents by sonication with a Branson-1510 ultrasonicator and filtered through a syringe filter (pore size: 5 μm) after sedimentation. Infrared spectroscopy was measured on a Nicolet 730 FT-IR spectrometer equipped with an attenuated total reflection (ATR) setup. The samples were deposited as pristine material on the diamond crystal and pressed on it with a stamp. Measurements with a scan number of 100 were recorded for each sample and the background was subtracted. For determining the concentration, GNR dispersions were passed through membrane filters with 200-nm pores and dried thoroughly under reduced pressure. For dispersions in high-boiling-point solvents, the filters were subsequently immersed for 1 day in dichloromethane and further dried under reduced pressure. The increase in the weight of the filers was carefully measured by using a microbalance (METTLER TOLEDO, MX5) to obtain the concentration of the dispersions.

Materials

Unless otherwise noted, materials were purchased from Fluka, Aldrich, Acros, ABCR, Merck, and other commercial suppliers and used as received. 1,3-Bis(6-bromo-[1,1'-biphenyl]-3-yl)propan-2-one[1], 3-[(triisopropylsilyl)ethynyl]benzil[2], 1-bromo-3-dodecylbenzene (**S1**)[3], and 1,3-bis(4-bromophenyl)propan-2-one (**S5**)[4] were prepared based on reported procedures.

Synthetic Procedures.

Monomers **1** and **3** were synthesized as displayed in Schemes S1 and S2, respectively.

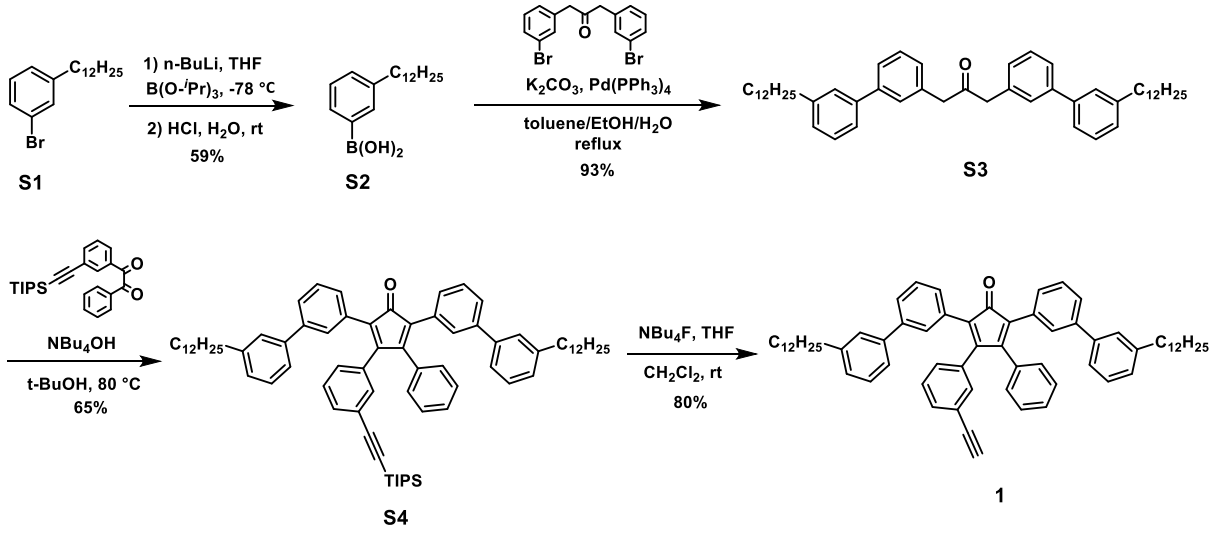

Scheme S1. Synthesis of monomer **1**.

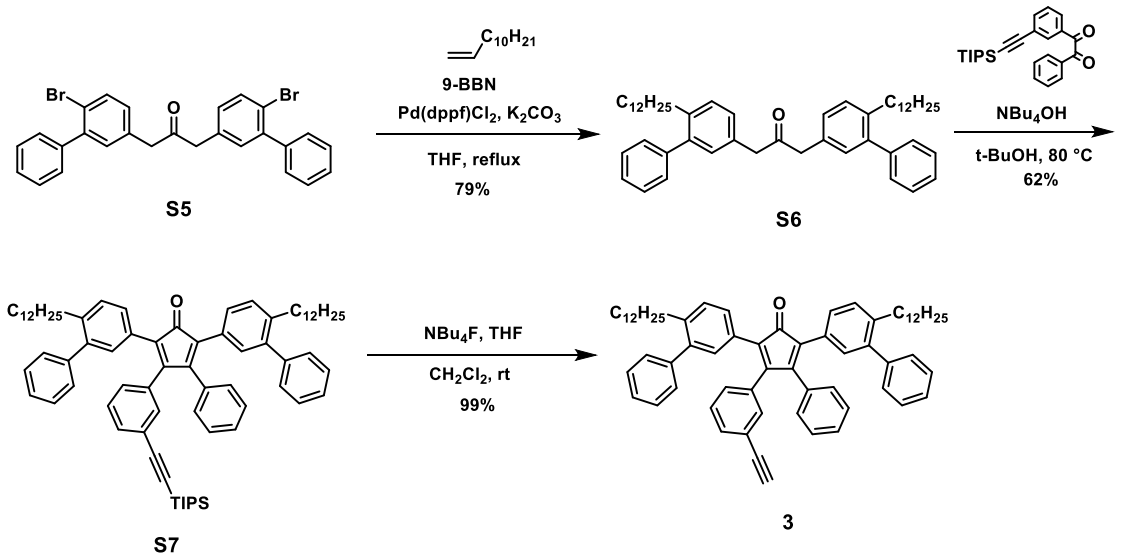

Scheme S2. Synthesis of monomer **3**.

3-Dodecylphenylboronic acid (S2)

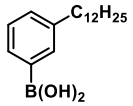

S2

To a cooled (–78°C) solution of 1-bromo-3-dodecylbenzene (**S1**) (2.89 g, 8.89 mmol) in dry tetrahydrofuran (30.0 mL) was added dropwise a solution of *n*-butyllithium (1.60 M in hexane, 6.40 mL, 10.2 mmol) under argon atmosphere. The mixture was stirred at the same temperature for 40 min, and then triisopropyl borate was added at –78°C. The reaction mixture was allowed to warm to room temperature overnight, and then stirred for 1 h with hydrochloric acid (2.0 M, 30.0 mL). The product was then extracted into ether, dried over sodium sulfate and evaporated. Purification by silica gel column chromatography (eluent: 50% ethyl acetate/hexane) gave the title compound as a white solid (1.51 g, 59% yield). ^{1}H NMR (250 MHz, CD_2Cl_2) δ 0.80 (t, J = 6.3 Hz, 3H), 1.18–1.23 (m, 18H), 1.47–1.54 (m, 2H), 2.54 (t, J = 7.5 Hz, 2H), 4.93 (s, 2H), 7.21–7.23 (m, 2H), 7.44–7.48 (m, 2H); ^{13}C NMR (75 MHz, CD_2Cl_2) δ 14.27, 23.08, 29.75, 29.90, 29.99, 30.03, 30.06, 32.06, 32.31, 36.29, 128.21, 131.08, 131.60, 134.00; MS (ESI, positive) *m/z* calcd for $C_{18}H_{31}BO_2$ $[M]^+$ 290.2, found 290.0.

1,3-Bis(3'-dodecyl-[1,1'-biphenyl]-3-yl)propan-2-one (S3)

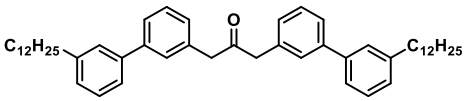

S3

To a degassed suspension of 1,3-bis(4-bromophenyl)propan-2-one (500 mg, 1.36 mmol), 3-dodecylphenylboronic acid (**S2**) (1.18 g, 4.07 mmol), and potassium carbonate (1.13 g, 8.18 mmol) in a mixture of toluene (70.0 mL), ethanol (17.5 mL), and water (17.5 mL) was added tetrakis(triphenylphosphino)palladium(0) (160 mg, 0.136 mmol). The reaction mixture was further degassed by argon bubbling for 10 min, and then refluxed for 7 h. After cooling to room temperature the aqueous layer was extracted three times with dichloromethane. The combined organic layers were washed three times with water and once with brine, dried over sodium sulfate, and evaporated. Purification by silica gel column chromatography (eluent: 5% ethyl acetate/hexane) gave the title compound as colorless oil (882 mg, 93% yield). ^{1}H NMR (250 MHz, CD_2Cl_2) δ 0.78 (t, J = 6.3 Hz, 6H), 1.17–1.24 (m, 36H), 1.49–1.60 (m, 4H), 2.55 (t, J = 7.5 Hz, 4H), 3.75 (s, 4H), 7.03–7.09 (m, 4H), 7.19–7.32 (m, 10H)), 7.38–7.42 (m, 2H); ^{13}C NMR (62.5 MHz, CD_2Cl_2) δ 13.87, 22.67, 29.34, 29.38, 29.51, 29.60, 29.63, 29.66, 31.65,

31.90, 35.98, 49.20, 124.30, 125.68, 127.16, 127.47, 128.33, 128.35, 128.55, 128.90, 134.67, 140.59, 141.69, 143.59, 205.19 (C=O); HRMS (ESI, positive) *m/z* calcd for $C_{51}H_{71}O$ $[M+H]^+$ 699.5505, found 699.5480.

2,5-Bis(3'-dodecyl-[1,1'-biphenyl]-3-yl)-3-phenyl-4-{3-[(triisopropylsilyl)ethynyl] phenyl} -2,4-cyclopentadienone (**S4**)

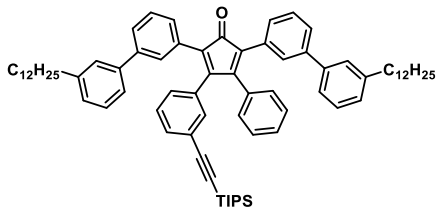

S4

To a degassed solution of 1,3-bis(3'-dodecyl-[1,1'-biphenyl]-3-yl)propan-2-one (**S3**) (727 mg, 1.04 mmol) and 3-[(triisopropylsilyl)ethynyl]benzil (667 mg, 1.71 mmol) in *tert*-butanol (29.0 mL) was added a solution of tetrabutylammonium hydroxide in methanol (40%, 0.440 mL, 0.0610 mmol) at 80 °C. After stirring at 80 °C for 40 min, the reaction was quenched by the addition of 2M hydrochloric acid, and extracted three times with dichloromethane. The combined organic layers were washed three times with brine, dried over sodium sulfate, and evaporated. Purification by silica gel column chromatography (eluent: 13% dichloromethane/hexane) gave the title compound as a purple sticky oil (712 mg, 65% yield). ^{1}H NMR (250 MHz, CD_2Cl_2) δ 0.78 (t, J = 6.3 Hz, 6H), 0.93–0.97 (m, 21H), 1.17–1.27 (m, 36H), 1.46–1.53 (m, 4H), 2.45–2.53 (m, 4H), 6.90–7.05 (m, 8H), 7.08–7.40 (m, 17H); ^{13}C NMR (62.5 MHz, CD_2Cl_2) δ 11.68, 14.35, 18.83, 23.14, 29.81, 29.86, 29.88, 30.00, 30.10, 30.14, 32.14, 32.17, 32.37, 36.42, 91.89 (Ar-C≡), 106.67 (≡C-TIPS), 123.86, 124.56, 124.63, 125.72, 126.09, 126.60, 126.86, 127.55, 127.62, 127.83, 128.55, 128.69, 128.88, 128.92, 128.95, 129.13, 129.27, 129.38, 129.65, 129.78, 131.36, 131.52, 132.04, 133.56, 133.75, 133.80, 140.98, 141.06, 141.28, 141.52, 143.98, 154.12, 155.36, 200.41 (C=O); HRMS (ESI, positive) *m/z* calcd for $C_{76}H_{97}OSi$ $[M+H]^+$ 1053.7309, found 1053.7319.

2,5-Bis(3'-dodecyl-[1,1'-biphenyl]-3-yl)-3-(3-ethynylphenyl)-4-phenyl-2,4-cyclopentadienone (**1**)

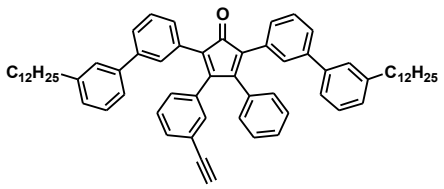

1

To a solution of 2,5-bis(3'-dodecyl-[1,1'-biphenyl]-3-yl)-3-phenyl-4-{3-[(triisopropylsilyl) ethynyl]phenyl}-2,4-cyclopentadienone (**S4**) (316 mg, 0.300 mmol) in dichloromethane (30.0 mL) was added with a solution of tetra-*n*-butylammonium fluoride in tetrahydrofuran (1.0 M, 0.900 mL, 0.900 mmol). After stirring at room temperature for 30 min, water was added to the reaction mixture. The resulting suspension was extracted three times with dichloromethane, and the combined organic layers were washed five times with water, dried over sodium sulfate, and evaporated at 40 °C. Purification by silica gel column chromatography (eluent: 14% dichloromethane/hexane) gave the title compound as a purple sticky oil (214 mg, 80% yield). ^{1}H NMR (250 MHz, CD_2Cl_2) δ 0.78 (t, J = 6.3 Hz, 6H), 1.17–1.24 (m, 36H), 1.48–1.53 (m, 4H), 2.47–2.54 (m, 4H), 2.96 (s, 1H), 6.92–7.05 (m, 8H), 7.09–7.40 (m, 17H); ^{13}C NMR (62.5 MHz, CD_2Cl_2) δ 14.32, 23.12, 29.78, 29.83, 29.87, 29.98, 30.07, 30.11, 31.01, 32.14, 32.19, 32.35, 36.39, 36.43, 78.19 (≡CH), 83.07 (Ar-C≡), 122.65, 124.55, 124.58, 125.67, 126.18, 126.63, 126.84, 127.53, 127.56, 127.83, 127.87, 128.69 , 128.78, 128.90, 128.94, 129.10, 129.26, 129.35, 129.65, 130.17, 131.21, 131.47, 132.51, 133.00, 133.56, 134.30, 140.96, 141.30, 143.99, 144.04, 154.09, 155.26, 200.36 (C=O); HRMS (ESI, positive) *m/z* calcd for $C_{67}H_{77}O$ $[M+H]^+$ 897.5974, found 897.5989.

Polyphenylene precursor 2

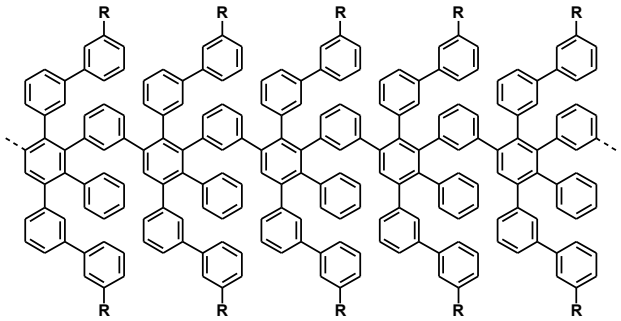

2: R = $C_{12}H_{25}$

A degassed solution of 2,5-bis(3'-dodecyl-[1,1'-biphenyl]-3-yl)-3-(3-ethynylphenyl)-4-phenyl-2,4-cyclopentadienone (**1**) (169 mg, 0.188 mmol) in diphenyl ether (0.850 mL, 221 mM) was

refluxed for 36 h using a heating mantle. The purple color disappeared and the solution turned pale yellow, indicating the completion of the polymerization. After cooling to room temperature, methanol was added. The precipitates were collected by filtration using a membrane filter to afford the crude polymer **2-SI** as a pale yellow solid (150 mg, 92% yield, M_w = 38000–72000, M_n = 11000–15000, PDI = 3.5–4.9 based on SEC analysis with PPP and PS standards). The crude polymer was dissolved in tetrahydrofuran, and reprecipitated with methanol (tetrahydrofuran/methanol = 2:1 in volume ratio). The precipitates were subsequently collected by filtration, and washed with a mixture of tetrahydrofuran and methanol (2:1 volume ratio). This process was repeated for five times to obtain precursor **2-I** (55.0 mg, 34% yield, M_w = 64000–125000, M_n = 47000–83000, PDI = 1.4–1.5; SEC analysis with PPP and PS standards). FTIR (powder) 3081, 3054, 3026, 2922, 2852, 1600, 1577, 1464, 1392, 1376, 890, 781, 700, 620 cm^{-1}; ^1H NMR (300 MHz, CD_2Cl_2) δ 0.74–0.78 (m, 6H), 1.15, (br, 36H), 2.47 (br, 4H), 6.53–6.94 (m, 26H).

6-CGNR-I

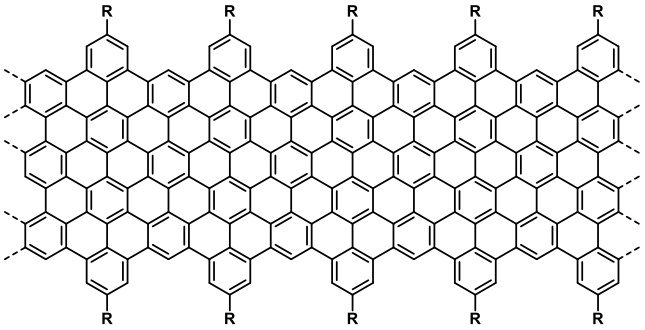

6-CGNR-I: R = $C_{12}H_{25}$

A solution of polyphenylene precursor **2-I** (10.2 mg) in unstabilized dichloromethane (40.0 mL) was degassed by argon bubbling for 10 min. To the above degassed solution was added a suspension of iron(III) chloride (266 mg, 1.64 mmol, 7.5 eq. for one hydrogen to be removed) in nitromethane (4.00 mL). After stirring at room temperature for 72 h under continuous bubbling with argon presaturated with dichloromethane, the reaction was quenched by addition of methanol to form bluish black precipitates. The precipitates were collected by filtration with a membrane filter, washed with methanol and tetrahydrofuran, and then sonicated for 30 min in tetrahydrofuran (50.0 mL). This process was repeated again to give **6-CGNR-I** as bluish black powder (7.60 mg, 76% yield). FTIR (powder) 2917, 2847, 1585, 1450, 1295, 1204, 1152, 864, 808, 718 cm^{-1}; Raman (powder, 532 nm) 3211, 2931, 2647, 1608, 1327 cm^{-1}.

1,3-Bis(2-dodecyl-[1,1'-biphenyl]-4-yl)propan-2-one (**S6**)

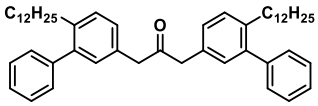

S6

A mixture of 1-dodecene (2.60 mL, 11.5 mmol) and a solution of 9-borabicyclo[3.3.1]nonane (9-BBN, 0.500 M in tetrahydrofuran, 23.0 mL, 11.5 mmol) was stirred for 6 h at room temperature, and then a degassed mixture of a solution of 1,3-bis(6-bromo-[1,1'-biphenyl]-3-yl)propan-2-one (**S5**) (1.00 g, 1.92 mmol) in tetrahydrofuran (40.0 mL) and an aqueous solution of potassium carbonate (1.50 M, 7.70 mL, 11.6 mmol) was added via cannula. [1,1′-Bis(diphenylphosphino) ferrocene] dichloropalladium ($Pd(dppf)Cl_2$, 210 mg, 0.287 mmol) was added to the resulting reaction mixture, which was then refluxed for 24 h. After cooling to room temperature, the aqueous layer was extracted for three times with dichloromethane. The combined organic layers were washed three times with water and once with brine, dried over sodium sulfate, and evaporated. Purification by silica gel column chromatography (eluent: 20% dichloromethane/hexane) gave the title compound as a white solid (1.17 g, 79% yield). ^{1}H NMR (250 MHz, CD_2Cl_2) δ 0.80 (t, J = 6.3 Hz, 6H), 1.08–1.22 (m, 36H), 1.31–1.37 (m, 4H), 2.44 (t, J = 7.5 Hz, 4H), 6.87 (d, J = 2.5 Hz, 2H), 6.98 (dd, J = 7.5, 2.5 Hz, 2H), 7.24–7.34 (m, 12H); ^{13}C NMR (75 MHz, CD_2Cl_2) δ 14.29, 23.10, 29.66, 29.76, 29.81, 29.87, 30.01, 30.05, 31.71, 32.33, 32.99, 49.07, 127.12, 128.34, 128.85, 129.58, 129.86, 131.48, 131.79, 139.49, 142.13, 142.40, 205.98 (C=O); HRMS (ESI, positive) *m/z* calcd for $C_{51}H_{72}O$ $[M+H]^+$ 699.5505, found 699.5478.

2,5-Bis(6-dodecyl-[1,1'-biphenyl]-3-yl)-3-phenyl-4-{3-[(triisopropylsilyl)ethynyl]phenyl}-2,4-cyclopentadienone (**S7**)

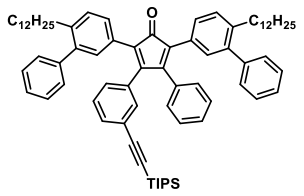

S7

To a degassed solution of 1,3-bis(4-dodecyl-[1,1':2',1"-terphenyl]-4'-yl)propan-2-one (**S6**) (624 mg, 0.933 mmol) and 3-[(triisopropylsilyl)ethynyl]benzil (600 mg, 1.54 mmol) in *tert*-butanol (28 mL) was added a solution of tetrabutylammonium hydroxide in methanol (40%, 1.33 mL, 0.187 mmol) at 80 °C. After stirring at 80 °C for 40 min, the reaction was quenched by the addition of 2 M hydrochloric acid, and extracted three times with dichloromethane.

The combined organic layers were washed three times with brine, dried over sodium sulfate, and evaporated. Purification by silica gel column chromatography (eluent: 13% dichloromethane/hexane) gave the title compound as a purple sticky oil (606 mg, 62% yield). ^{1}H NMR (300 MHz, CD_2Cl_2) δ 0.79 (t, J = 6.0 Hz, 6H), 0.98–1.04 (m, 21H), 1.08–1.18 (m, 36H), 1.32–1.37 (m, 4H), 2.39–2.48 (m, 4H), 6.82 (dt, J = 7.5, 1.3 Hz, 1H), 6.90–6.95 (m, 3H), 7.00–7.27 (m, 21 H); ^{13}C NMR (62.5 MHz, CD_2Cl_2) δ 11.67, 14.33, 18.83, 23.13, 29.68, 29.79, 29.86, 29.89, 29.93, 30.02, 30.05, 30.08, 31.63, 32.36, 33.18, 33.26, 91.61 (Ar-C≡, 106.79 (≡C-TIPS), 123.64, 125.52, 125.78, 127.05, 128.20, 128.28, 128.32, 128.44, 128.47, 128.88, 129.29, 129.37, 129.42, 129.55, 129.65, 129.82, 131.92, 132.12, 133.48, 133.78, 133.86, 140.34, 140.63, 141.74, 141.91, 142.04, 142.07, 153.36, 154.64, 200.85 (C=O); HRMS (ESI, positive) *m/z* calcd for $C_{76}H_{96}OSi$ $[M+H]^+$ 1053.7309, found 1053.7318.

2,5-Bis(6-dodecyl-[1,1'-biphenyl]-3-yl)-3-(3-ethynylphenyl)-4-phenyl-2,4-cyclopentadienone (**3**)

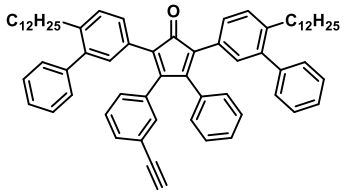

3

To a solution of 2,5-bis(6-dodecyl-[1,1'-biphenyl]-3-yl)-3-phenyl-4-{3-[(triisopropylsilyl) ethynyl]phenyl}-2,4-cyclopentadienone (**S7**) (245 mg, 0.233 mmol) in dichloromethane (30 mL) was added a solution of tetra-*n*-butylammonium fluoride in tetrahydrofuran (1.00 M, 0.780 mL, 0.780 mmol). After stirring at room temperature for 30 min, water was added to the reaction mixture. The resulting suspension was extracted three times with dichloromethane, and the combined organic layers were washed five times with water, dried over sodium sulfate, and evaporated at 40 °C. Purification by silica gel column chromatography (eluent: 17% dichloromethane/hexane) gave the title compound as a purple sticky oil (208 mg, 99% yield). ^{1}H NMR (300 MHz, CD_2Cl_2) δ 0.78 (t, J = 7.5 Hz, 6H), 1.08–1.23 (m, 36H), 1.32–1.37 (m, 4H), 1.32–1.37 (m, 4H), 2.40–2.46 (m, 4H), 2.59 (s, 1H) 6.85–6.93 (m, 5H), 7.02–7.30 (m, 20H); ^{13}C NMR (75 MHz, CD_2Cl_2) δ 14.32, 23.12, 29.68, 29.78, 29.82, 29.85, 29.89, 30.02, 30.07, 31.57, 31.60, 32.35, 33.18, 77.97 (≡CH), 83.17 (Ar-C≡), 122.40, 125.44, 125.94, 127.07, 128.13, 128.28, 128.30, 128.40, 128.48, 128.55, 128.86, 129.29, 129.38, 129.46, 129.54, 129.64, 130.19, 132.04, 132.09, 132.28, 133.05, 133.65, 134.34, 140.39, 140.60,

141.76, 141.89, 142.02, 153.36, 154.57, 200.81 (C=O). HRMS (ESI, positive) *m/z* calcd for $C_{67}H_{78}O$ $[M+H]^+$ 897.5974, found 897.5961.

Polyphenylene precursor 4

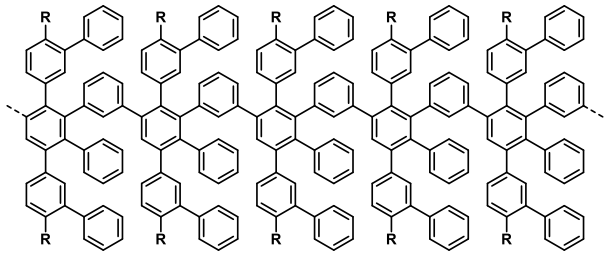

4: R = $C_{12}H_{25}$

A degassed solution of 2,5-bis(6-dodecyl-[1,1'-biphenyl]-3-yl)-3-(3-ethynylphenyl)-4-phenyl-2,4-cyclopentadienone (**3**) (198 mg, 0.221 mmol) in diphenyl ether (1.00 mL, 221 mM) was refluxed for 58 h using a heating mantle. The purple color disappeared and the solution turned pale yellow, indicating the completion of the polymerization. After cooling to room temperature, methanol was added. The precipitates were collected by filtration using a membrane filter to afford the crude polymer **4-SI** as a pale yellow solid (170 mg, 89% yield, M_w = 47000–91000, M_n = 15000–21000, PDI = 3.1–4.3 based on SEC analysis with PPP and PS standards). The crude polymer was fractionalized by using recycling reparative SEC system (Japan Analytical Industry JAIGEL-2H+2.5H, eluent: chloroform, 3.0 mL/min) to remove low-molecular-weight fractions, affording 39 mg (20% yield) of precursor **4-I** with M_w of 61000–121000, M_n of 40000–68000, and PDI of 1.6–1.8 based on SEC analysis. The rest of polymer fractions were separated again by using recycling reparative SEC to yield precursor **4-II** (10 mg, 5% yield) with M_w of 64000–125000, M_n of 43000–75000, and PDI of 1.5–1.7 based on SEC analysis. FTIR (powder) 3081, 3057, 3024, 2923, 2852, 1600, 1577, 1488, 1463, 1456, 1442, 1377, 1072, 892, 830, 768, 699, 629; ^{1}H NMR (300 MHz, CD_2Cl_2) δ 0.78–1.16 (m, 46H), 2.37 (br, 4H), 6.53–7.21 (m, 26H).

6-CGNR-II

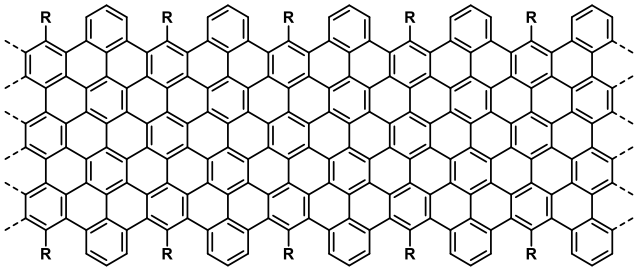

6-CGNR-II: R = $C_{12}H_{25}$

A solution of polyphenylene precursor **4-I** (22.0 mg) in unstabilized dichloromethane (80.0 mL) was degassed by argon bubbling for 10 min. To the degassed solution was added a suspension of iron(III) chloride (574 mg, 3.54 mmol, 7.5 eq. for one hydrogen to be removed) in nitromethane (9.00 mL). After stirring at room temperature for 72 h under continuous bubbling with argon presaturated with dichloromethane, the reaction was quenched by addition of methanol to form bluish black precipitates. The precipitates were collected by filtration with a membrane filter, washed with methanol and tetrahydrofuran, and then sonicated for 30 min in tetrahydrofuran (50 mL). This process was repeated again to give **6-CGNR-II** as bluish black powder (20.4 mg, 96% yield): FTIR (powder) 2918, 2848, 1585, 1451, 1175, 866, 810, 754, 718, 700 cm^{-1}; Raman (powder, 532 nm) 3192, 2906, 2631, 1595, 1308 cm^{-1}.

Characterizations of polyphenylene precursors

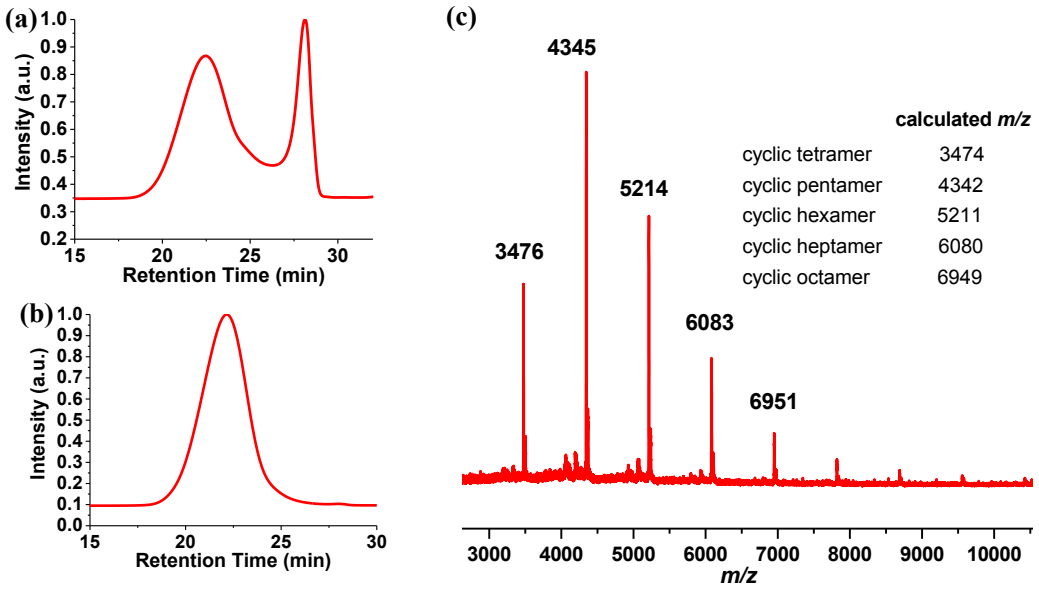

Figure S1. (a), (b) Normalized SEC profiles of polyphenylene precursors (a) **2-SI** and (b) **2-I** (eluent: THF, 1.0 mL/min, UV detector). (c) MALDI-TOF MS analysis of a low-molecular-weight fraction of precursor **2** obtained during the SEC fractionation (reflectron mode, matrix: TCNQ). The shoulders of the peaks correspond to $[M + Na]^+$ and peaks due to the fragmentation of alkyl chains are also visible. Inset: calculated *m*/*z* of cyclic oligomers.

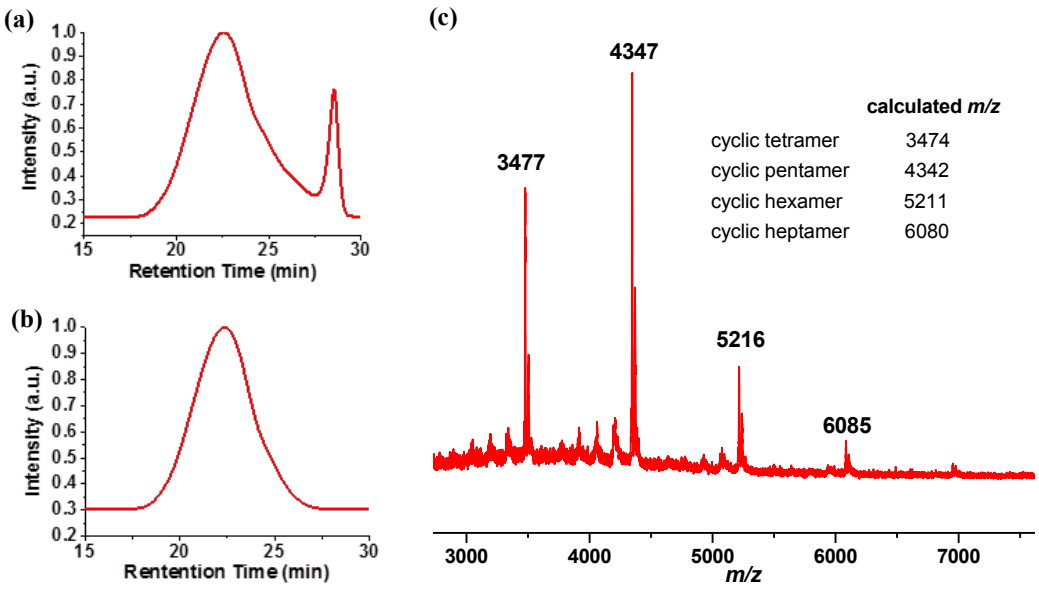

Figure S2. (a), (b) Normalized SEC profiles of polyphenylene precursors (a) **4-SI** and (b) **4-I** (eluent: THF, 1.0 mL/min, UV detector). (c) MALDI-TOF MS analysis of a low-molecular-weight fraction of precursor **4** obtained during the SEC fractionation (reflectron mode, matrix: TCNQ). The shoulders of the peaks correspond to $[M + Na]^+$ and peaks due to the fragmentation of alkyl chains are also visible. Inset: calculated *m*/*z* of cyclic oligomers.

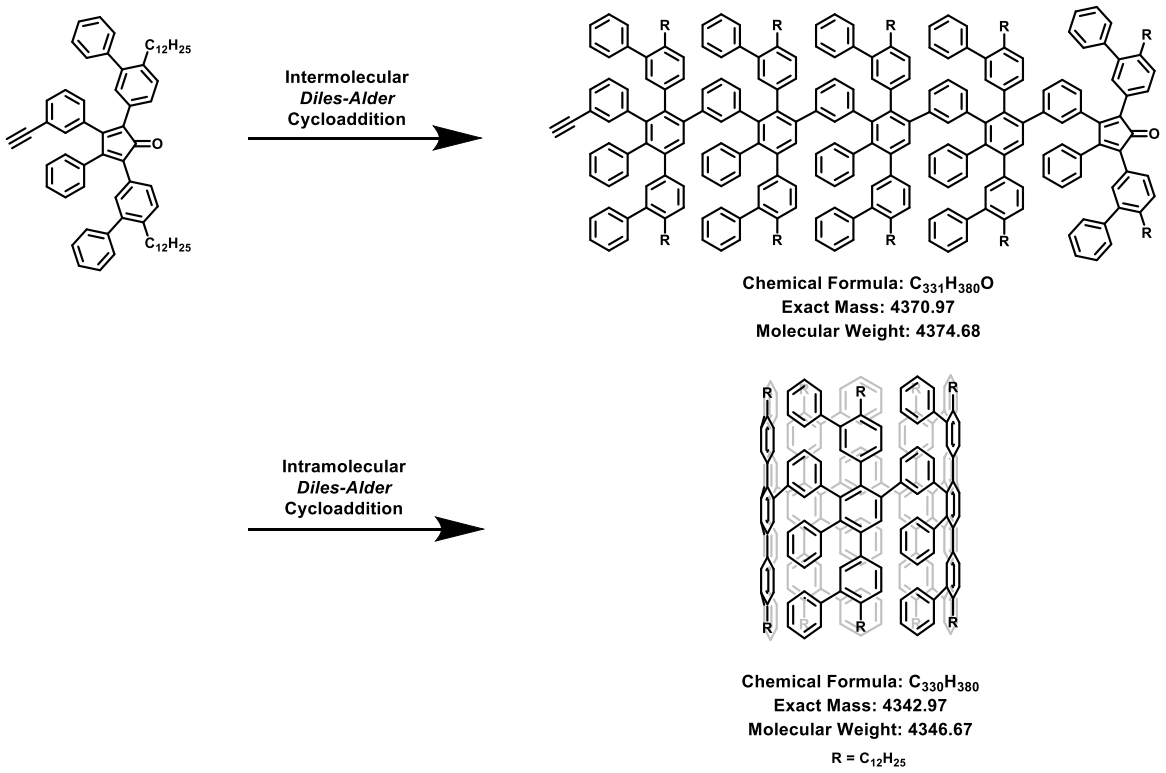

Figure S3. Proposed formation of cyclic oligomers through intramolecular Diels–Alder cycloaddition of linear oligomers as represented by the formation of cyclic pentamer via linear pentamer.

Ab initio simulations.

Theoretical methodology.

Simulations of the ground-state structural and vibrational properties were performed using a first-principle supercell implementation of Density-Functional Theory (DFT) and Density-Functional Perturbation Theory (DFPT)[5] based on plane waves and pseudopotentials, as available in the Quantum ESPRESSO package.[6] Calculations were performed by employing LDA exchange correlation (xc) functional and norm-conserving pseudopotentials, with a cutoff energy for the wavefunctions of 70 Ry. To mimic isolated GNRs with periodic boundary conditions, a vacuum region of about 12 Å was added in the directions perpendicular to GNR longitudinal axis so as to avoid fictitious interactions with the system replicas. The atomic positions within the cell were fully relaxed until forces were less than 5×10^{-4} Ry$\cdot$ bohr^{-1}, while the lattice constant along the GNR longitudinal axis was optimized separately. Structural properties and phonon frequencies were calculated using a 16×1×1 k-point grid to sample the Brillouin zone.

The Kohn-Sham band structure obtained for the optimized geometry was improved by introducing many-body corrections within the G_0W_0 approximation for the self-energy operator.[7] Here, the dynamic dielectric function was obtained within the plasmon-pole approximation,[8] by employing a box-shaped truncation of the Coulomb potential[9] to remove the long-range interaction between periodic images. The optical absorption spectrum was then computed as the imaginary part of the macroscopic dielectric function starting from the solution of the Bethe-Salpeter (BS) equation, which allows for the inclusion of electron-hole interaction effects.[7] The static screening in the direct term was calculated within the random-phase approximation (RPA) with inclusion of local field effects; the Tamm-Dancoff approximation for the BS Hamiltonian was employed. The aforementioned *GW*-BS calculations were performed by using the YAMBO code.[10]

To make the calculations of electronic, optical and vibrational properties more affordable, we chose to use shorter alkyl chains for the edge functionalization (ethyl or butyl groups instead of docecyl chains). The effect of the chain length on the properties of interest is analysed in the following. Moreover, the chains were placed in out-of-plane configuration, where chains on opposite edges were chosen to point in opposite directions with respect to the plane containing the GNR backbone. The investigation of the effect of these type of choices on the vibrational properties of GNRs has been extensively described elsewhere,[11] and is here limited to the IR spectra in the region of interest.

Effect of structural distortions and chain length on the electronic properties.

GNRs decorated with C_4H_9 chains were calculated and their atomic positions were fully optimized according to the procedure described above. The DFT band structures obtained for these systems are shown in Figure 4, solid turquoise line. The comparison with the band structure of GNRs passivated with shorter chains, i.e. C_2H_5 (magenta crosses), shows nearly no difference, indicating that the chain length does not influence the electronic properties in the region of interest. In view of these results, the functionalization with C_2H_5 is then adopted for the *GW*-BS calculations shown in the main article.

In order to evaluate the impact of structural distortions induced by the alkyl chains, we considered the two systems (6-CGNR-I and -II) as resulting from full structural optimization in presence of C_4H_9 chains, removed the alkyl chains, and substituted them with monoatomic H. The coordinates of the added H atoms were fully optimized while leaving the rest of the structure frozen. The band structures of these modified GNRs, shown by black plus in Figure S4, indicate that the bangap change from 6-CGNR-I to 6-CGNR-II is mainly accounted for by

the distortion of the C backbone. In fact, the band inversion between the lowest two conduction bands going from 6-CGNR-I to 6-CGNR-II is already present when only the distortion is taken into account, and could be understood by looking at the corresponding single-particle orbitals at the Γ point: in fact, distorsions affect the most the energies of those states having charge localized on the buckled C atoms at the edge (*c2* for 6-CGNR-I and *c1* for 6-CGNR-II in Figure S4).

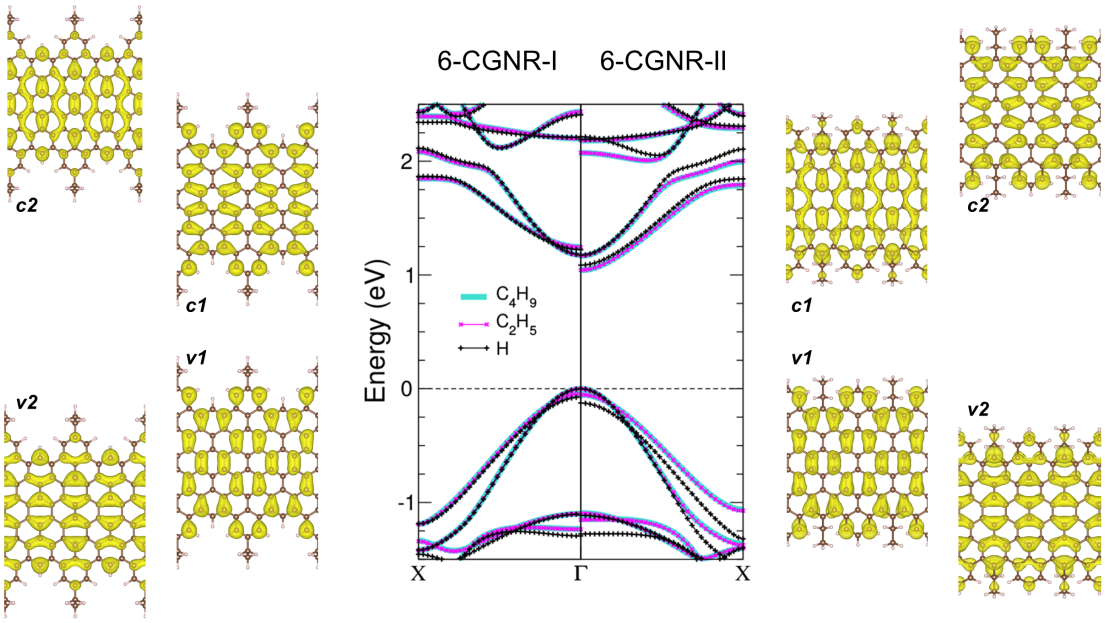

Figure S4. DFT band structure of 6-CGNR-I and 6-CGNR-II, as modelled by using alkyl chains of different length (i.e. C_2H_5 and C_4H_9). The impact of the structural distortion is evaluated by comparing the systems with H passivation only (black plus). Single-particle orbitals at the Γ point are displayed for the two highest valence bands (*v1*, *v2*) and for the two lowest conduction bands (*c1*, *c2*).

Effect of chain length on the GNR vibrational properties and phonon mode analysis.

Figure S5a shows the IR spectra for the four GNRs described in the main text. 4-CGNR and 8-CGNR display very similar spectra in the region 700–900 cm^{-1}, with two main features: the rocking of the CH_2 groups of the chains, which appears at ~712 cm^{-1}, and the SOLO mode at 862 cm^{-1}. The rocking mode appears at the same frequency also for 6-CGNR-I, while it is redshifted to 683 cm^{-1} in the case of 6-CGNR-II. Instead, another mode of different nature (involving both chains and carbon backbone) appears in the spectrum of 6-CGNR-II at about the same frequency of the rocking of 6-CGNR-I. SOLO modes are found for 6-CGNR-I at 839 and 859 cm^{-1}, while an additional mode, though not edge specific, is present at 786 cm^{-1}.

The 6-CGNR-II spectrum can be mainly distinguished for the prominent TRIO mode at about 762 cm^{-1}. At variance with 6-CGNR-I, several structures appear in the range 700–750 cm^{-1} and 800–870 cm^{-1}, but they are not edge-specific.

The effect of the chain length on the IR spectra was investigated in a selected case (i.e. 8-CGNR). As shown in Figure S5b, the main features characterizing the IR spectra are mostly captured by using a butyl functional group (red curve).

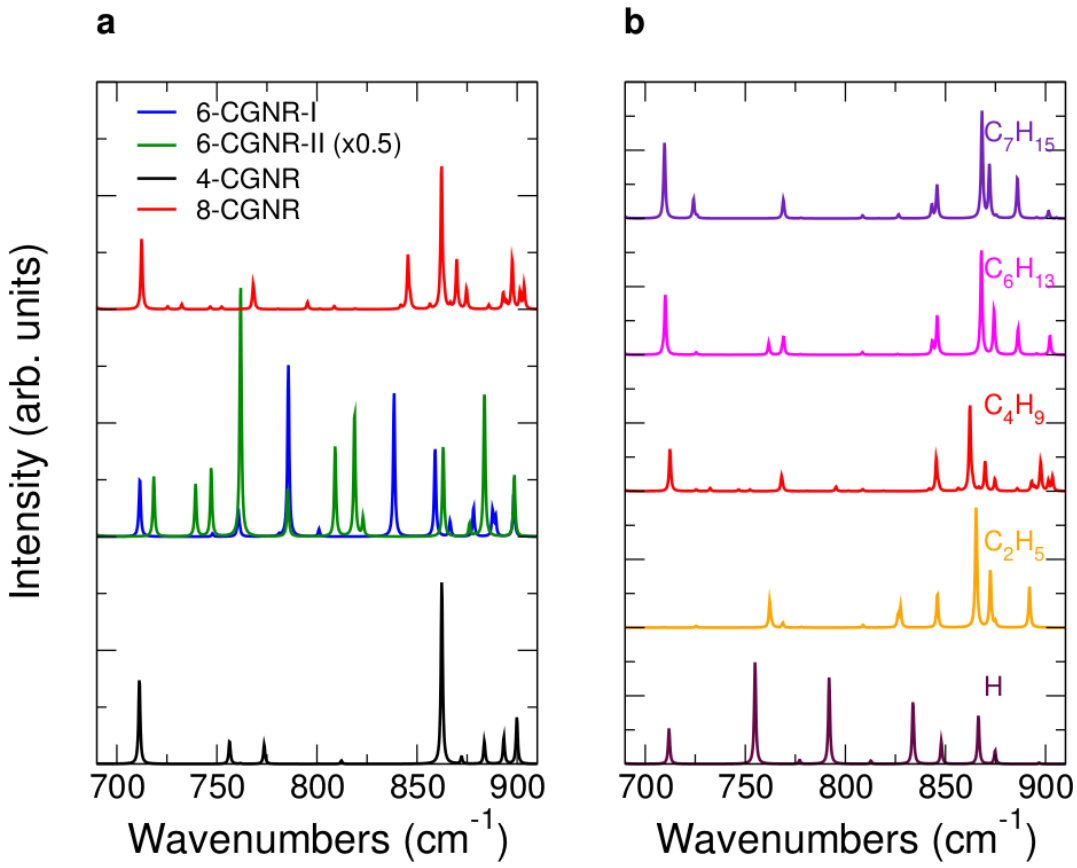

Figure S5. a) IR spectra for 6-CGNR-I/II, 4-CGNR, and 8-CGNR. b) For 8-CGNR, the impact of the chain length on the IR spectra is evaluated comparing the results obtained for different chain lengths as well as for H passivation.

FTIR analysis of precursors and GNRs

FTIR spectrum of precursor **2** revealed the strong attenuation of the signals assigned to aromatic C–H stretching vibrations at 3081, 3054, and 3026 cm^{-1}, as well as out-of-plane (*opla*) C–H stretching vibrations at 890, 781, and 700 cm^{-1} characteristic of mono- and di-substituted benzene rings after the cyclodehydrogenation (Figure S6). Similar band attenuations were also observed in the case of precursor **4** after planarization to 6-CGNR-II. These results were in line with the FTIR characterizations of previously solution-synthesized GNRs,[1, 12] corroborating the successful syntheses of 6-CGNR-I/II.

The rocking mode of the CH groups of the chains appeared at 718 cm^{-1} for 6-CGNR-I, similar to those of 4-CGNR (720 cm^{-1}) and 8-CGNR (718 cm^{-1})[1, 12](Figure S5a). Although this mode was predicted to redshift to 683 cm^{-1} in the case of 6-CGNR-II, another mode of different nature appeared in the spectrum of 6-CGNR-II at about the same frequency of the rocking of 6-CGNR-I, involving both chains and carbon backbone, as envisaged by the theoretical calculations, making it difficult to distinguish the specific edge morphology. Other differences can be noted in the region between 720 and 760 cm^{-1} and below 700 cm^{-1}, where additional peaks appear in the case of 6-CGNR-II only.

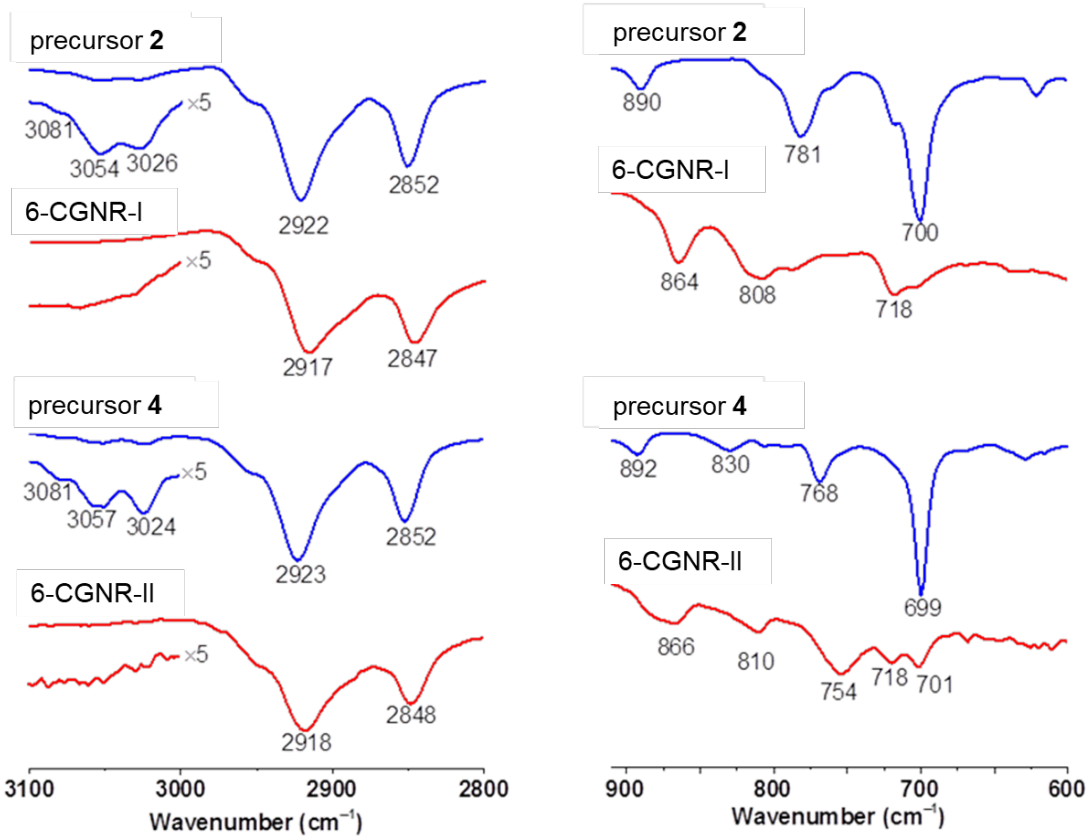

Figure S6. FTIR spectra of precursors **2**, precursor **4**, 6-CGNR-I, and 6-CGNR-II.

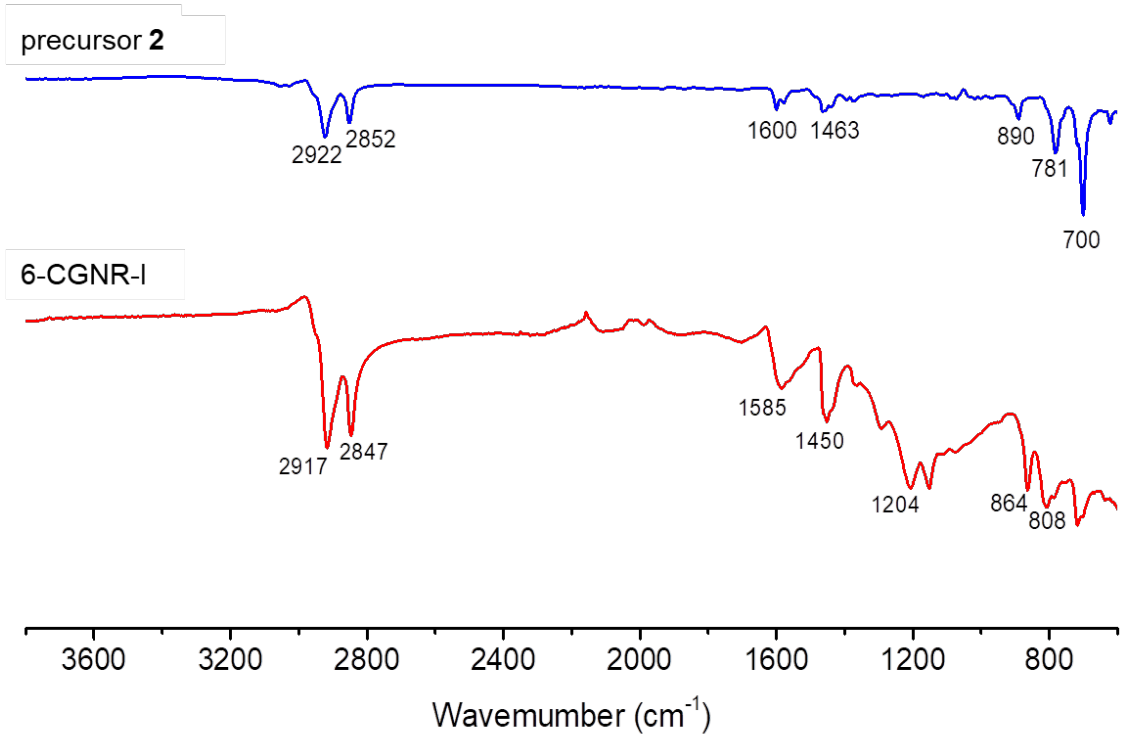

Figure S7. FTIR full spectra of polyphenylene precursor **2** and 6-CGNR-I.

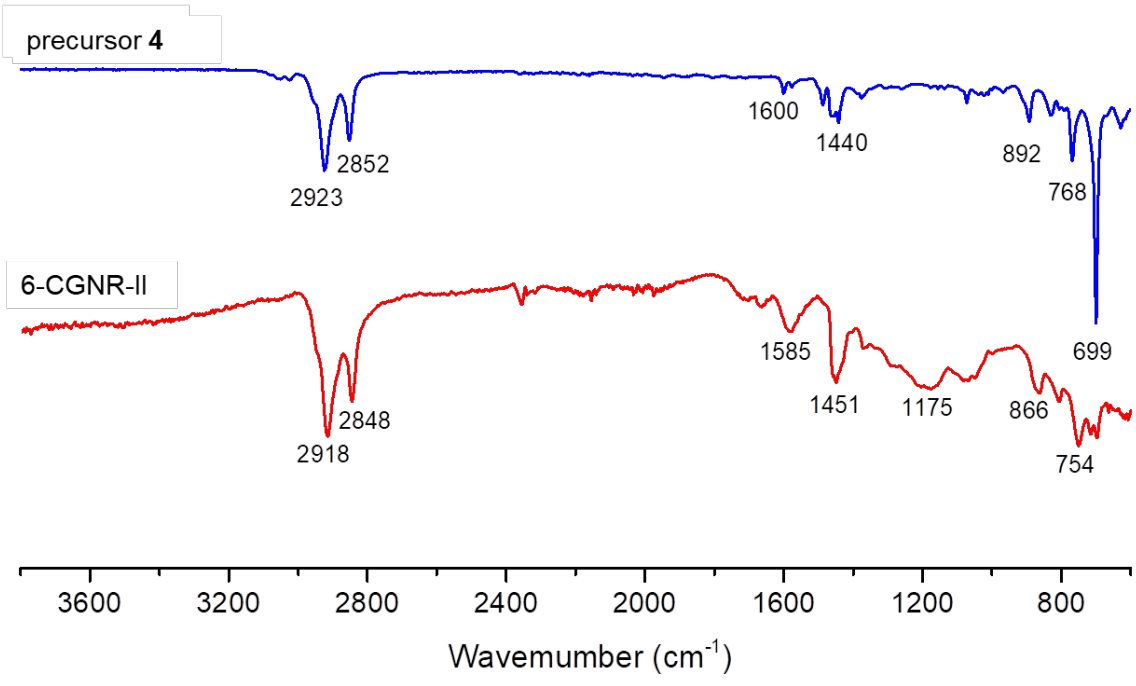

Figure S8. FTIR full spectra of polyphenylene precursor **4** and 6-CGNR-II.

Raman spectroscopy analysis of GNRs

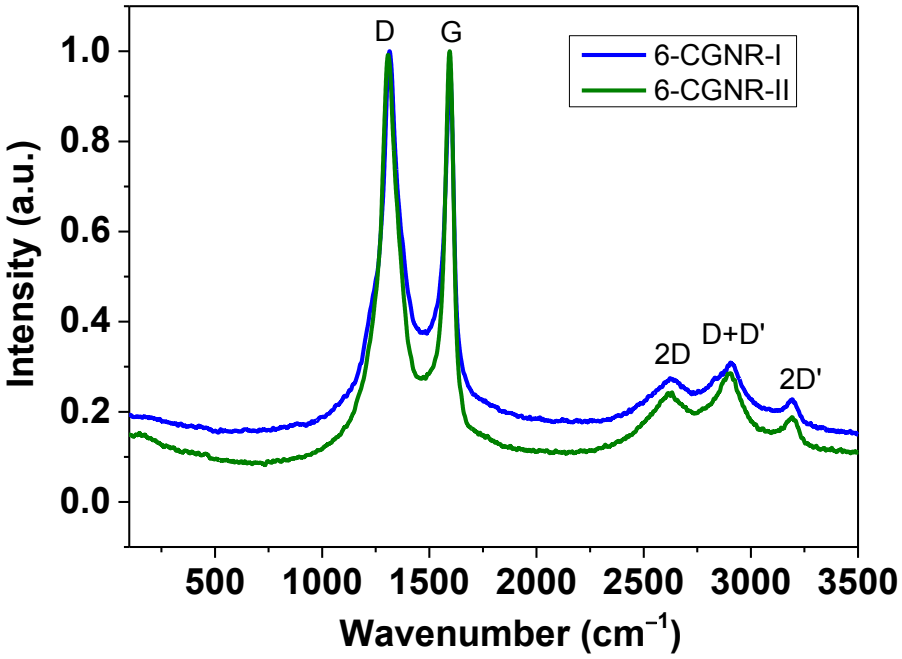

Figure S9. Raman spectra of 6-CGNR-I/II (powder, 532 nm).The intense first-order D and G peaks as well as second-order peaks are characteristic of GNRs.

Solid-state NMR analysis of GNRs

All solid-state magic-angle-spinning (MAS) spectra were acquired on a 16.4 T (700 MHz for ^{1}H) spectrometer using a 1.3 mm Bruker probe operating in double-resonance mode. The MA setting was done on KBr.[12] The MAS frequency was set to either 50000 or 59524 Hz, giving rotor periods of 16.8 and 20 μs, respectively. In the ^{1}H -^{1}H double quantum-single quantum (DQ-SQ)[13-14] correlation experiments, DQ recoupling and DQ reconversion were set to one rotor period. The dwell time in the indirect dimension was a rotor period and a full phase-cycle scheme of 16 scans was implemented. The carrier on ^{1}H was set at 4 ppm relative to tetramethylsilane (TMS) using adamantane as a secondary reference.[15-16] A 90 degree flip pulse was set to 1.5 μs (radio-frequency (rf) field strengths of ca. 167 kHz) in the experiments on GNR-cove and to 1.8 μs (rf field strength of ca. 139 kHz) in the experiments on GNR-edge. Recoupled polarization heteronuclear single quantum correlation (^{13}C{^{1}H} REPT-HSQC) experiments were used to probe the resonances of the ^{13}C nuclei. The recycling delay was set to 2 s in all experiments. All ^{1}H and ^{13}C{^{1}H} MAS NMR experiments were performed under ambient conditions. Processing was done in Topspin. Phase correction was done manually and windowing functions were imposed. In the ^{1}H -^{1}H DQ-SQ spectra, we have only used zeroth order phase correction. Very little zeroth order phase correction was needed in the

indirect dimension. A Gaussian multiplication using a line broadening parameter of –20 was applied and the fraction parameter was set such that the windowing maximum was approximately in the middle of the active fid.

2D solid-state ^{1}H–^{1}H double-quantum–single-quantum (DQ-SQ) NMR correlation spectroscopy was employed to probe the spatial proximity between the protons present at the edges of the GNRs for further characterization of 6-CGNR-I/II (Figure S10). Both 2D ^{1}H–^{1}H DQ-SQ NMR correlation spectra show significant broadening caused by the planarization of the polyphenylene precursors **2** and **4** as the protons become a part of the extended π-conjugated systems of 6-CGNR-I/II with heterogeneous solid-state packing. ^{1}H–^{1}H cross-correlations between the aliphatic and aromatic protons appear at the sum of the chemical shifts in the indirect (DQ) dimension and are illustrated by the horizontal line marked by the red/blue-green interaction circles in Figure S9a,c. A clear split ridge could be observed along the diagonal at higher ppm values in both spectra, indicating two types of aromatic protons that are in close proximity with each other. Accordingly, the lower and higher frequency parts of the aromatic signals could be assigned to the side (red circle) and the inner (blue circle) protons in 6-CGNR-I, respectively (Figure S10c), which is in agreement with the previously published assignment on similar GNR. Whereas, in the case of 6-CGNR-II, the aromatic signals with lower and higher ppm-values could be assigned to the outer (red circle) and side (blue circle) protons, respectively (Figure S10a). Figures S11 and S12 display the 1D $^{13}C\{^{1}H\}$ recoupled polarization heteronuclear single quantum correlation (REPT-HSQC) MAS NMR characterization of 6-CGNR-I/II and their precursors **2** and **4**, respectively. In the $^{13}C\{^{1}H\}$ REPT-HSQC spectrum of precursors **2** and **4**, two main regions can be assigned to the signals of the aromatic carbons at ca. 145-121 ppm ($^{13}C_{aromatic}$) and the aliphatic carbons at ca. 38 –20 ppm ($^{13}C_{aliphatic}$). In the aromatic region, we expect the signals at lower field at ca. 141 ppm to originate from quaternary carbons anchoring the aliphatic chain, the signals at ca. 132 from quaternary carbons embedded in the aromatic system, and the signals at ca. 127 ppm from aromatic carbons with protons. In the aliphatic region, we assign the signals at ca. 37 ppm to carbons adjacent to the anchoring point, the signals at ca. 30 to carbons in the aliphatic chain, and the signals ca. 23.5 ppm to methyl carbons. These assignments are based on the chemical shifts values and the intensities of the peaks. Addressing the GNRs, we likewise assign the signals of the aromatic carbons at ca. 150–112 ppm ($^{13}C_{aromatic}$) and the aliphatic carbons at ca. 45–4 ppm ($^{13}C_{aliphatic}$). We observe signals from the quaternary carbons at ca. 141 ppm. The ^{13}C signals of the GNRs are broadened compared to those of the precursor, indicating that the carbons are a part of an extended π-conjugated system with heterogeneous packing. We

conclude that the overall, the quality of both 6-CGNR-I and 6-CGNR-II is comparable to graphene nanoribbons that have been reported previously in the literature.[1, 17]

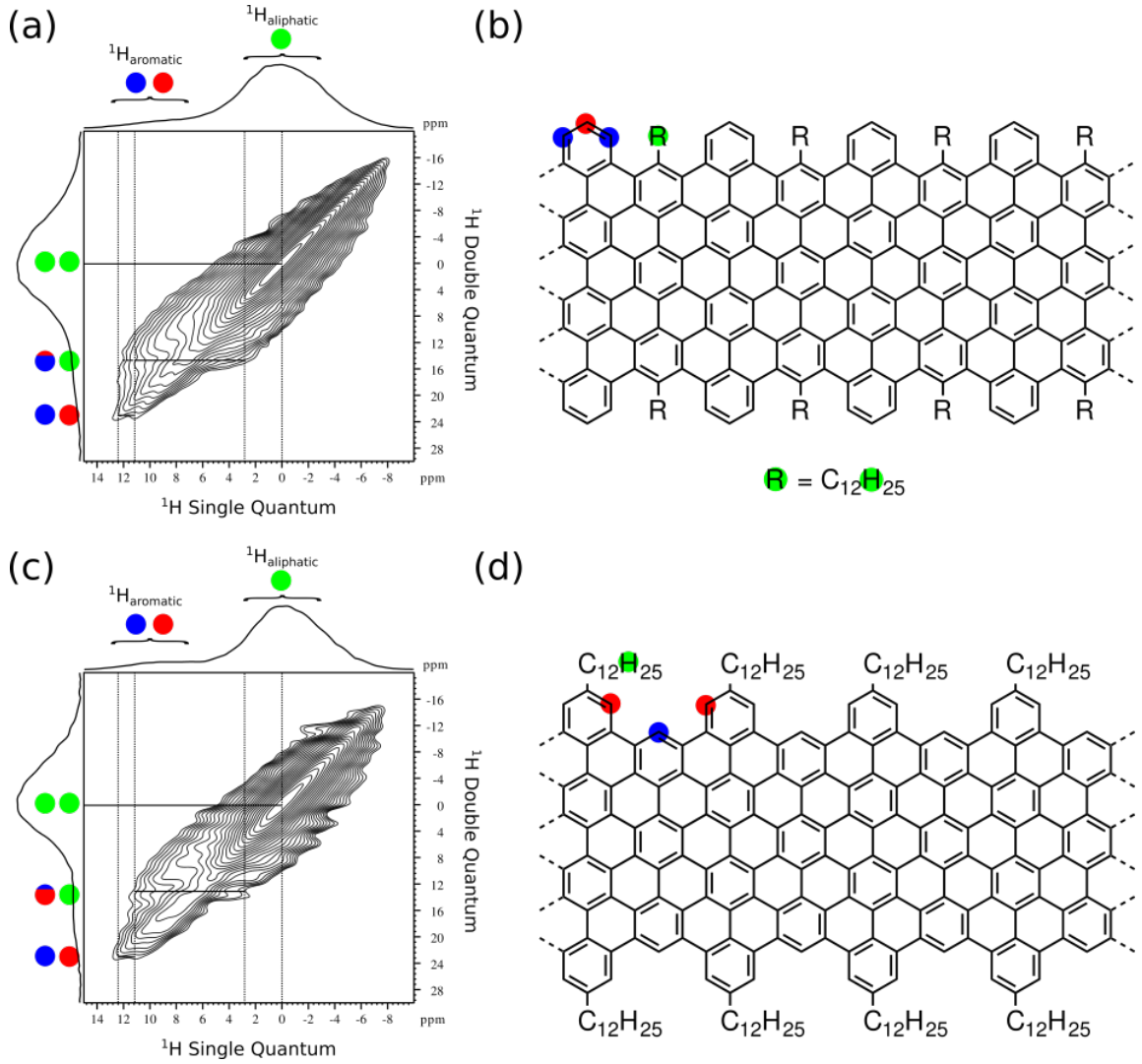

Figure S10. Solid-state ^{1}H NMR characterization of 6-CGNR-I/II. The 2D ^{1}H-^{1}H DQ-SQ correlation spectra of 6-CGNR-I (c) and 6-CGNR-II (a) were recorded at 16.4 T using MAS frequency of 59524 and 50000 Hz, respectively, with one rotor period of DQ recoupling. The regions marked by curly brackets illustrate the broad range of ^{1}H chemical shifts resulting from a heterogeneous packing. (b, d) Assignment scheme.

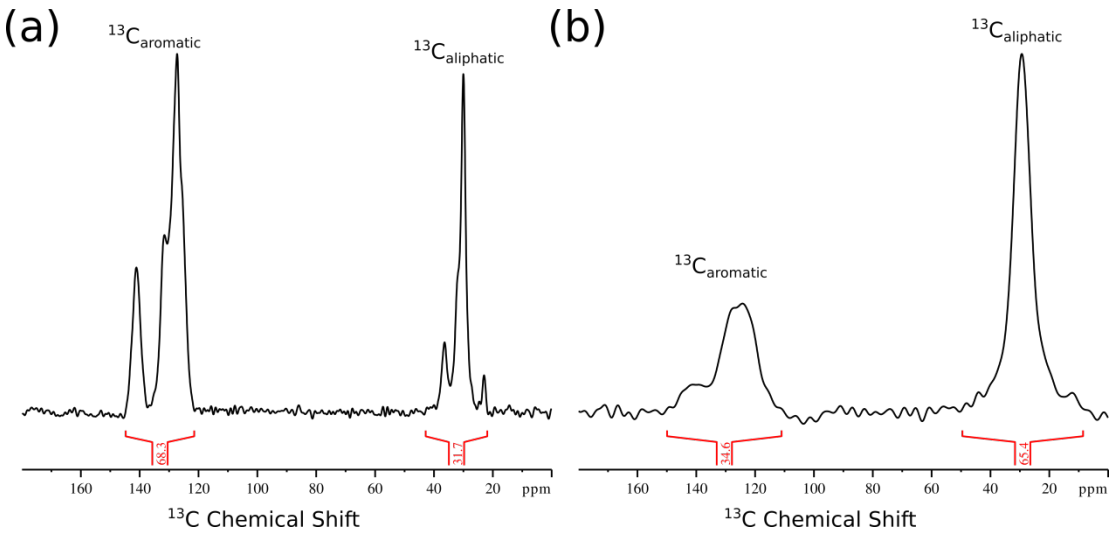

Figure S11. Solid-state $^{13}C\{^{1}H\}$ REPT-HSQC MAS NMR characterization of (a) 6-CGNR-I and (b) precursor **2** recorded at 16.4 T and MAS frequency of 59524 Hz. The REPT-HSQC used four rotor periods of REDOR recoupling.

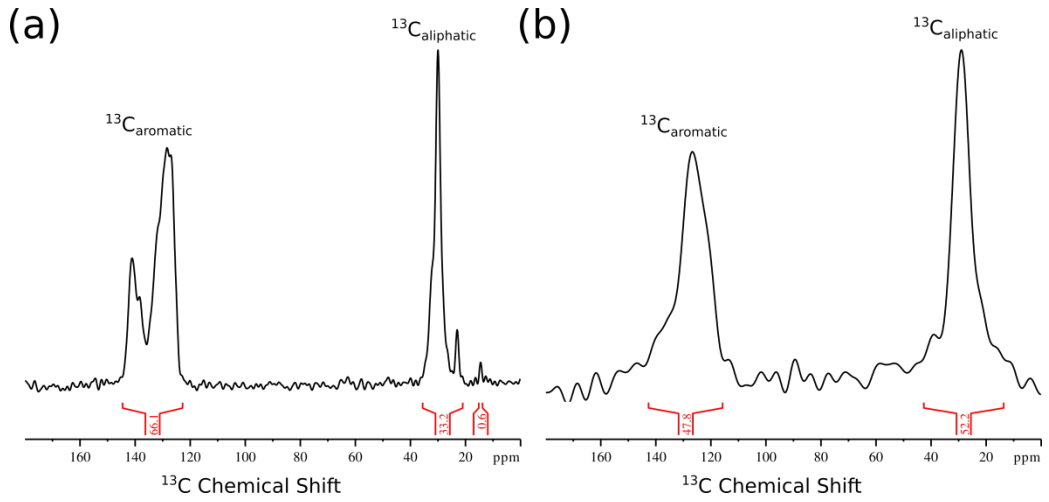

Figure S12. Solid-state $^{13}C\{^{1}H\}$ REPT-HSQC MAS NMR characterization of (a) 6-CGNR-II and (b) precursor **4** recorded at 16.4 T and MAS frequency of 50000 Hz. The REPT-HSQC used four rotor periods of REDO.

Photoluminescence excitation spectroscopy (PLE)

PLE spectroscopy was performed using a supercontinuum laser (Fianium) filtered by a monochromator (Ropers Scientific SP2150i) in the range 450–750nm, and by an AOFT filter in the range 700–950nm. The data recorded with the two excitation sources have been glued at 750 nm. The luminescence is dispersed in spectrometer (Ropers Scientific SP2300i) and detected with a CCD (Ropers Scientific PIXIS 100B). For both GNRs, the PLE is recorded by

monitoring the luminescence intensity on the low energy tail of the PL spectrum as a function of the excitation wavelength. The signal is then normalized by the number of incident photons.

Surface optical spectroscopic analysis of the GNRs

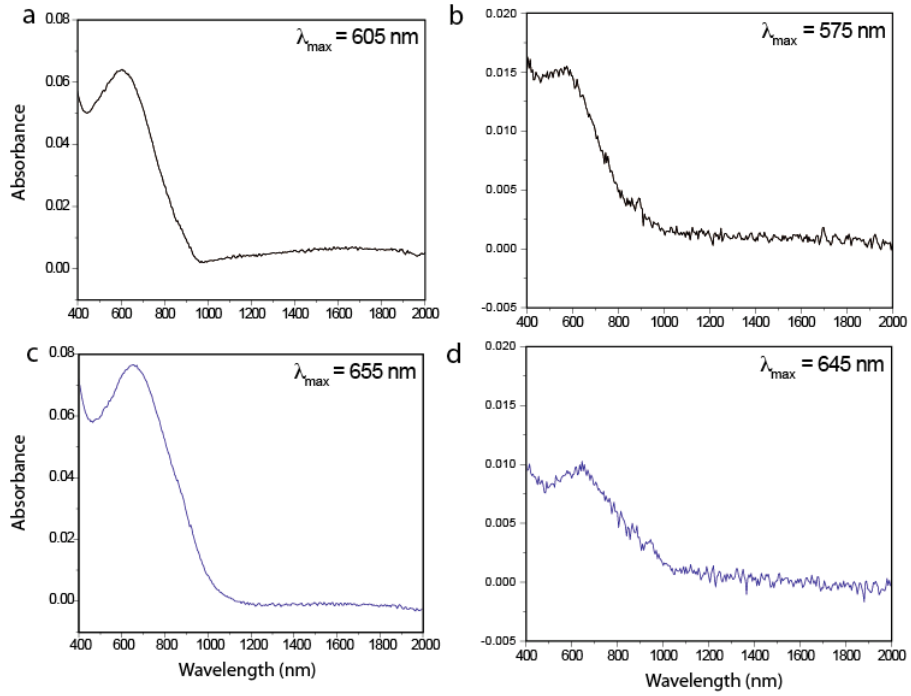

Figure S13. UV-vis-NIR absorption spectra of drop-casted GNR films. (a) 6-CGNR-I bulk films measured before ultrasonication. (b) 6-CGNR-I multilayers measured after ultrasonication. (c) 6-CGNR-II bulk films measured before ultrasonication. (d) 6-CGNR-II multilayers measured after ultrasonication.

STM and STS measurements

The STM/STS tips were prepared by etching a Pt/Ir wire (80%:20%, Goodfellow, UK). STM data were analyzed with the Gwyddion software.[39] The experiments were performed with a high purity diamond plate (Element Six, lateral dimensions: 4.5 × 4.5 mm, thickness: 500 μm). For the STS measurements, diamond substrates were cleaned with a piranha solution, acetone, isopropanol and oxygen plasma. The O-C(100) termination was prepared via oxygen microwave plasma (TePla 100-E): 300 s at 200 W load coil power and oxygen pressure of 1.4 mbar. The GNR solution in 1,2,4-trichlorobenzene (TCB, Sigma) was drop-casted onto the O-C(100) diamond and rinsed with isopropanol. The amount of GNR left on the surfaces was monitored via a UV/VIS/NIR Spectrometer, Lambda 900 (Perkin Elmer) measuring at 5 nm data interval, 0.32 and 0.68 s integration time for UV–vis and NIR, averaged 10 times. After GNR processing, the counter electrodes for the STS measurements were prepared as follows.

The GNR/diamond substrates were spin-coated with photoresist (AZ5214E) at 6000 RPM for 40 s and baked at 110 °C for 1 min. The samples were exposed to UV light through a chromium lithographic mask in a 200 W mask aligner for 2 s. After the first exposure, the samples were baked in air at 125 °C for 2 min. Then, the samples were exposed to UV light in the mask aligner for 30 s. The resist was developed in a bath mixture, AZ400k developer:water = 1:4, and then were rinsed in distilled water, followed by N_2 drying. The electrodes were made by evaporating 10 nm titanium and 30 nm gold onto the diamonds. Metal lift-off proceeded with acetone, isopropanol, and a water bath. For recovering the bare diamonds, the electrodes were removed by the hydrochloric acid (HCl, 36%, VWR) and nitric acid (HNO_3, 69%, VWR) at 80 °C for 1 h, followed by concentrated sulfuric acid (H_2SO_4, 96%, VWR) with potassium nitrate (KNO_3, Merck Millipore) at 220 °C for 1 hour. For the STM measurements, the O-C(100) substrates (see above) were converted to conductive H-C(100) in a quartz tube reactor (Seki Technotron Corp.) of a microwave-coupled ASTEX plasma system with three steps: 750 W and 50 mbar hydrogen pressure at a constant hydrogen flow rate of 100 SCCM (standard cubic centimeter per minute) at 700 °C for 15 min; 230 W, 10 mbar hydrogen pressure, 100 SCCM at 300 °C for 10 minutes; and 0 W, 10 mbar hydrogen pressure, 100 SCCM at 35 °C for 30 min.

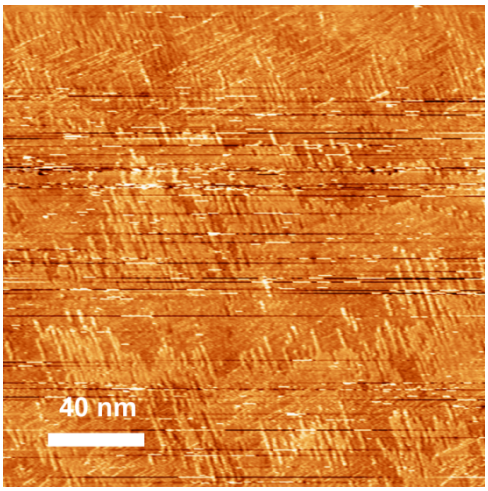

Figure S14. STM data of multilayers. 6-CGNR-II drop-casted on the surface of H-C(100) diamond. V_s = 300 mV, I_t = 30 pA.

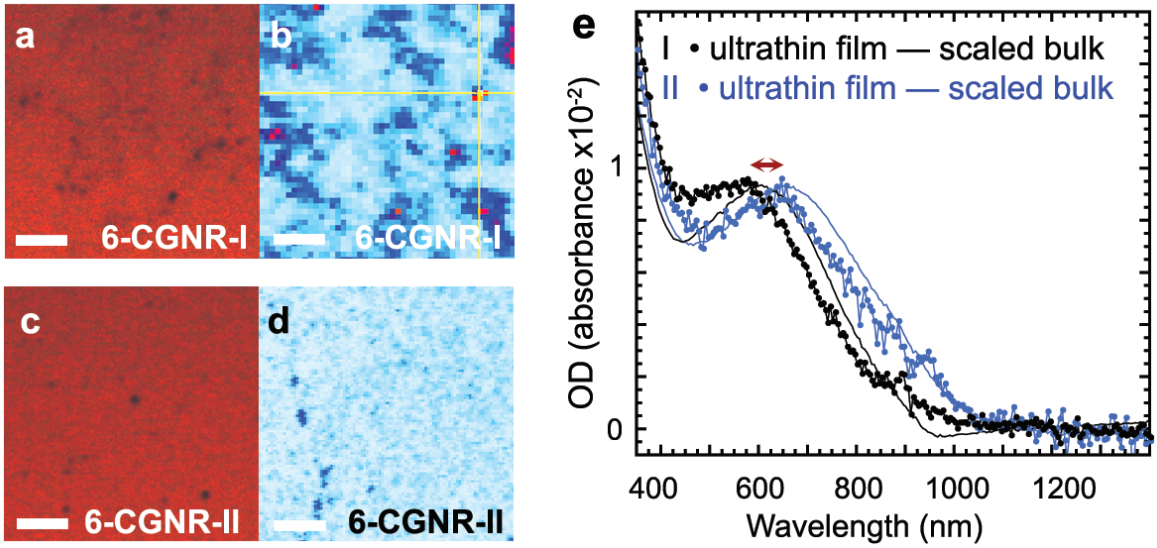

Figure S15. Optical characterization of GNR multilayers. Optical (a,c) and Raman (b,d) microscopy of 6-CGNR-I (a,b) and 6-CGNR-II (c,d) multilayers on diamond substrates. (e,f) (i) UV-vis-NIR absorption spectrum measured on thin and bulk films of O-C(100). The bulk films were scaled down a factor of ~10. The spectrum of 6-CGNR-I was also scaled down 20% for ease of comparison. Scale bar 4 μm.

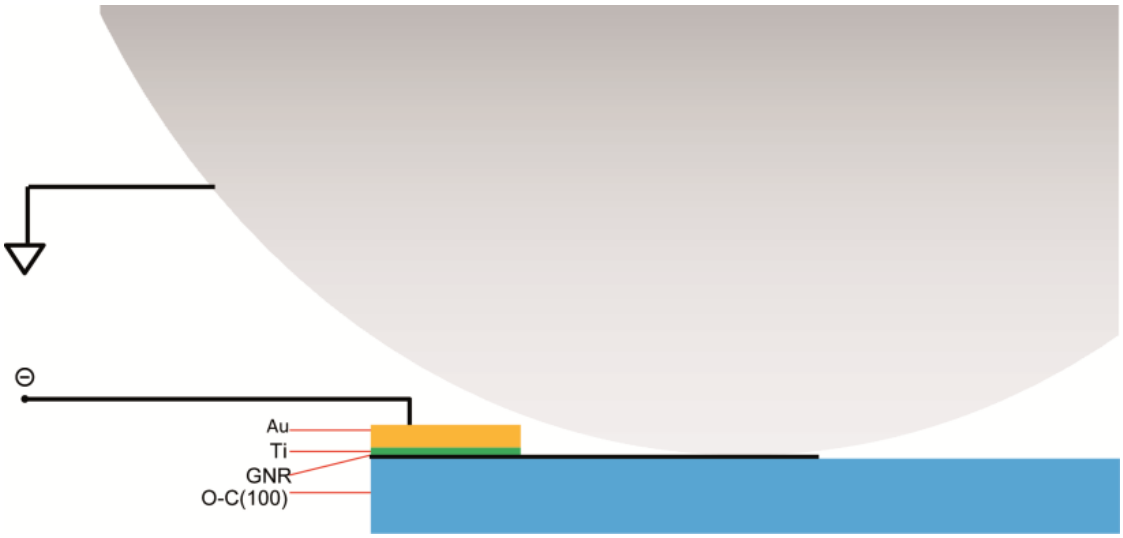

Figure S16. Schematics of the STS setup employed. An etched Pt-Ir STM tip is approached close to Au/Ti contacts. The scheme shows a thickness of gold, titanium and GNR films of 30 nm, 10 nm and ~1 nm respectively.

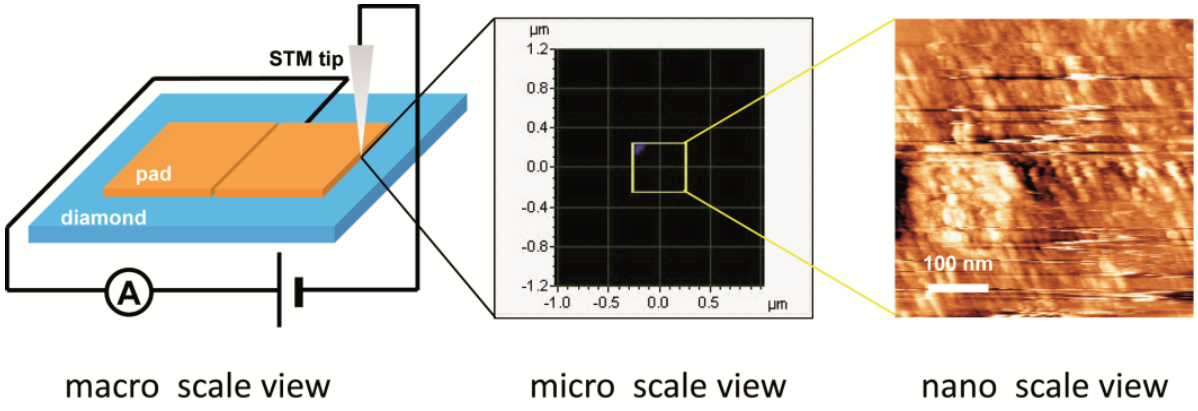

Figure S17. Working principle of the STS setup employed, depicting tunneling microscopy data of 6-CGNR-II near to the low contact-resistance Au/Ti electrode at typical parameters V_s = mV, I_t = pA. After a suitable GNR multilayer is identified by STM, STS is measured at >10 positions at the nanoscale, for >10 microscale positions, for at least 3 different macroscopic tip tunneling junctions close to the gold electrodes.

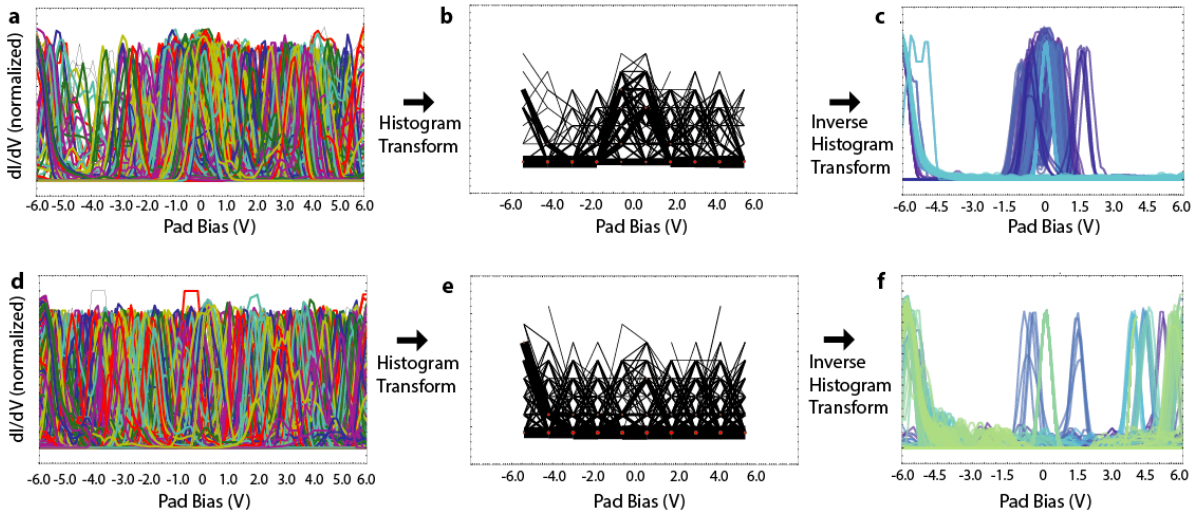

Figure S18. Total STS data collected and automatic histogram filtering. (a,d) The total data collected for 6-CGNR-II (a-c) and 6-CGNR-I (d-f) is normalized and then (b,e) binned in a network histogram. (c,f) The histogram is employed as a filter to extract and automatically color sets of data which share more than five histogram bins.

^{1}H and ^{13}C NMR spectra

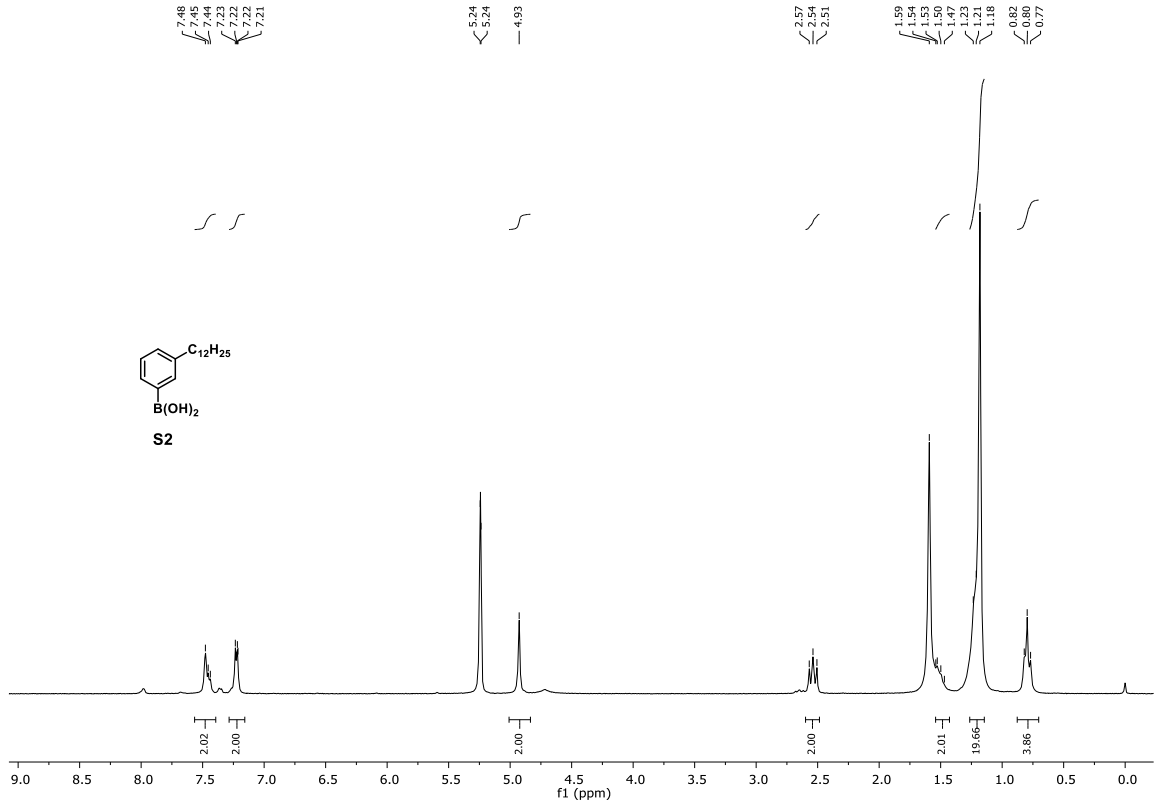

Figure S19. ^{1}H NMR spectrum of compound **S2** (250 MHz, CD_2Cl_2).

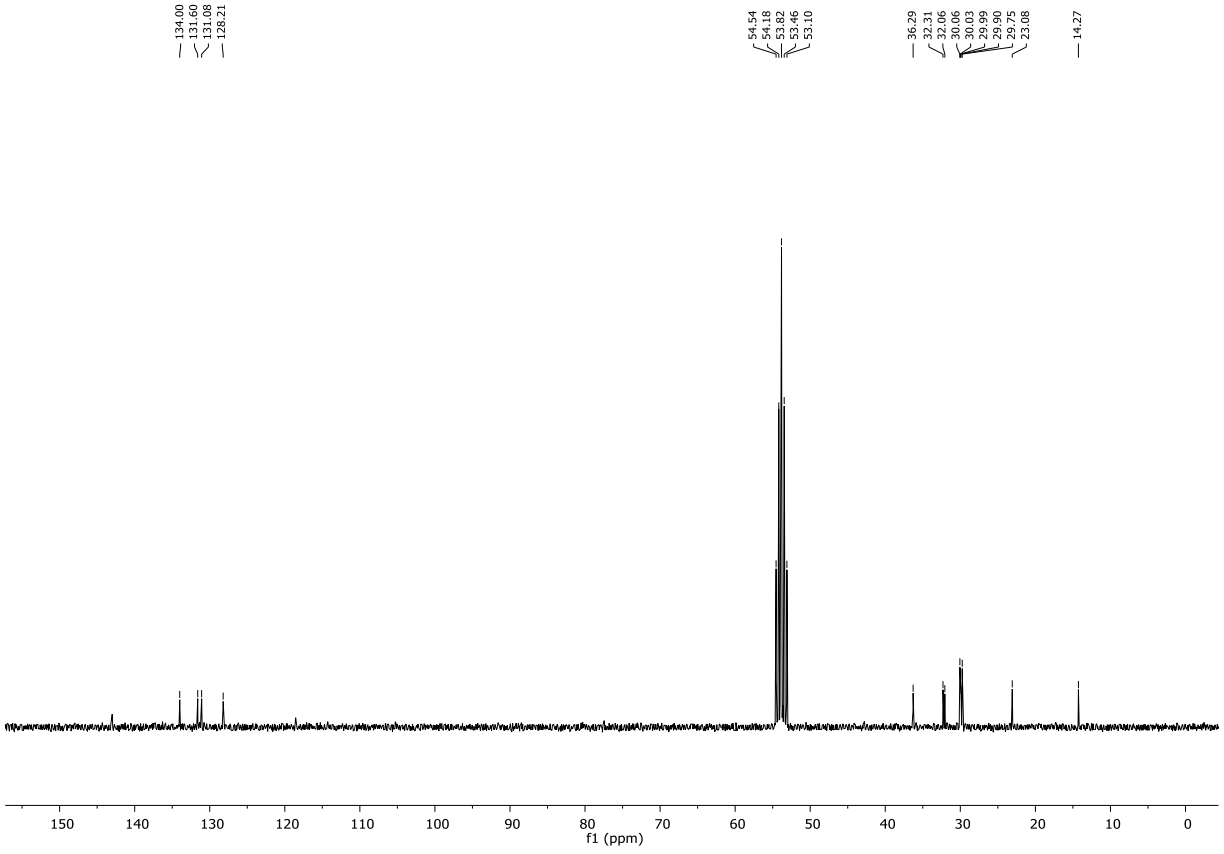

Figure S20. ^{13}C NMR spectrum of compound **S2** (75 MHz, CD_2Cl_2).

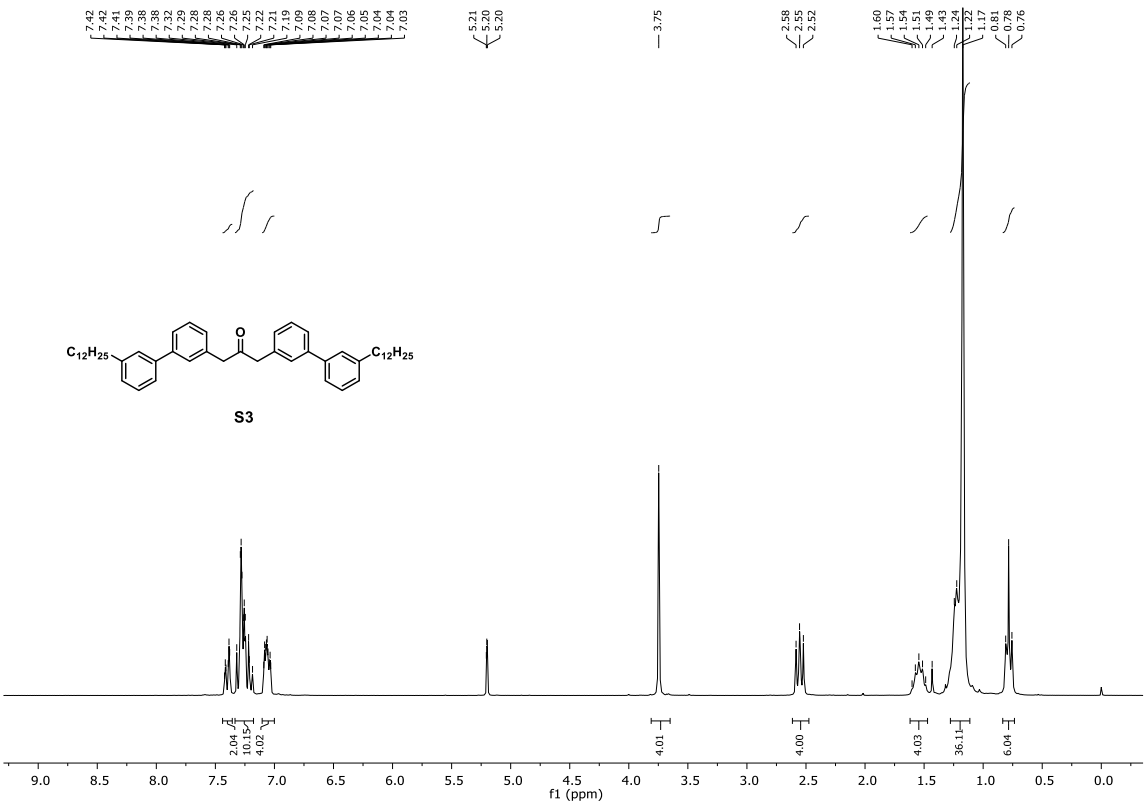

Figure S21. ^{1}H NMR spectrum of compound **S3** (250 MHz, CD_2Cl_2).

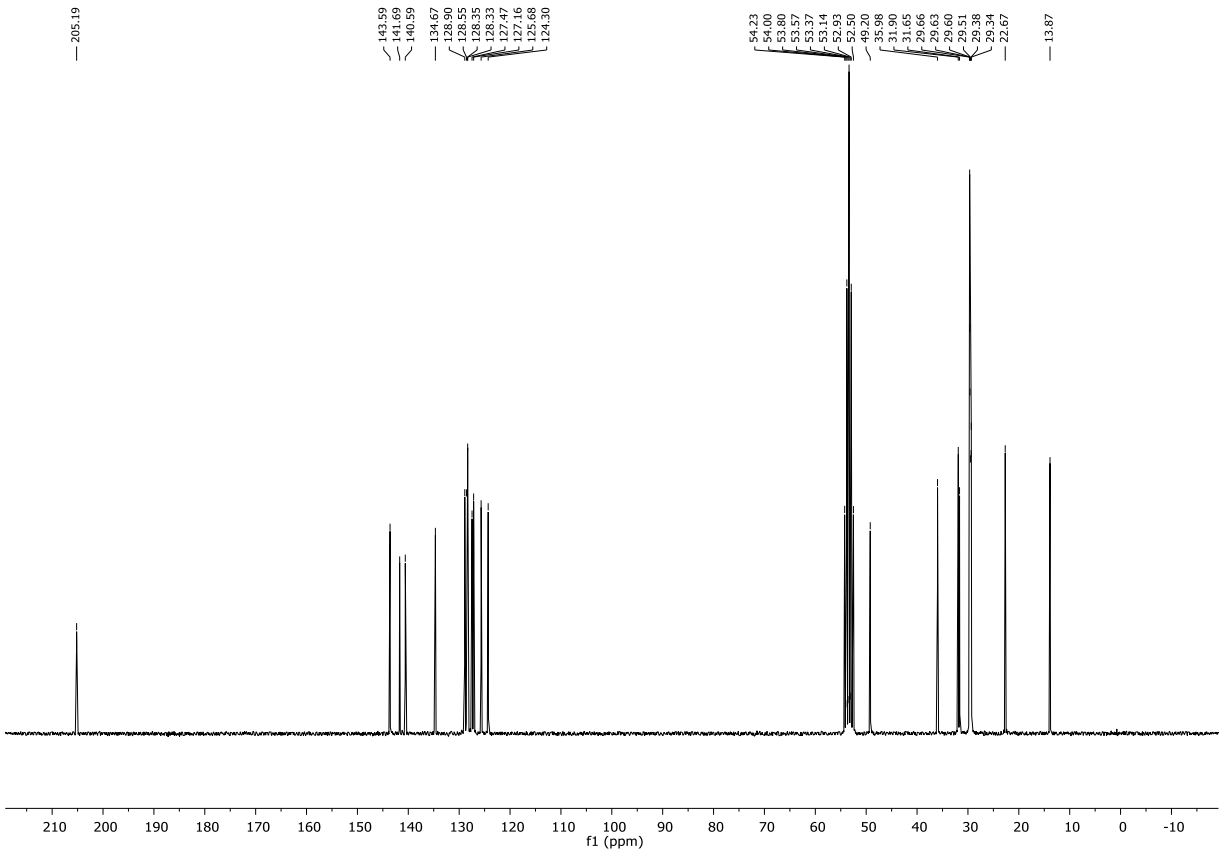

Figure S22. ^{13}C NMR spectrum of compound **S3** (62.5 MHz, CD_2Cl_2).

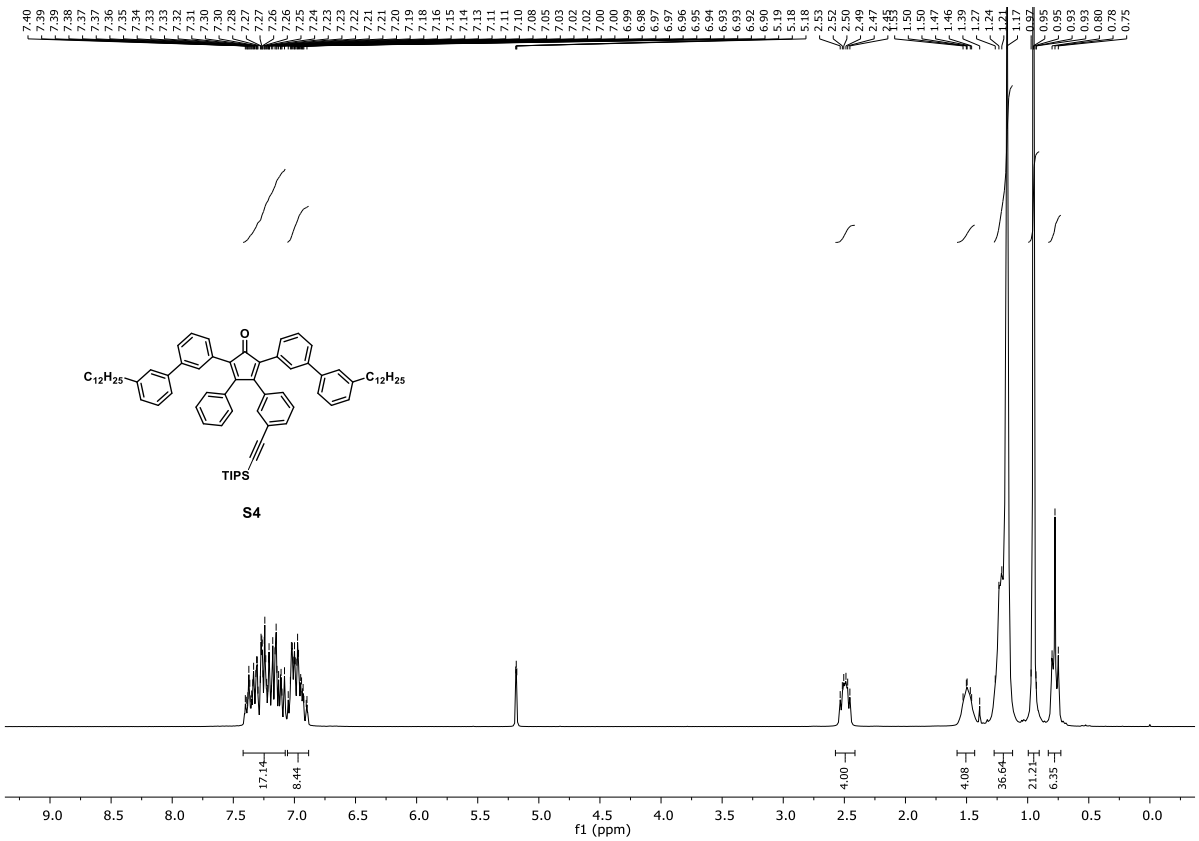

Figure S23. ^{1}H NMR spectrum of compound **S4** (250 MHz, CD_2Cl_2).

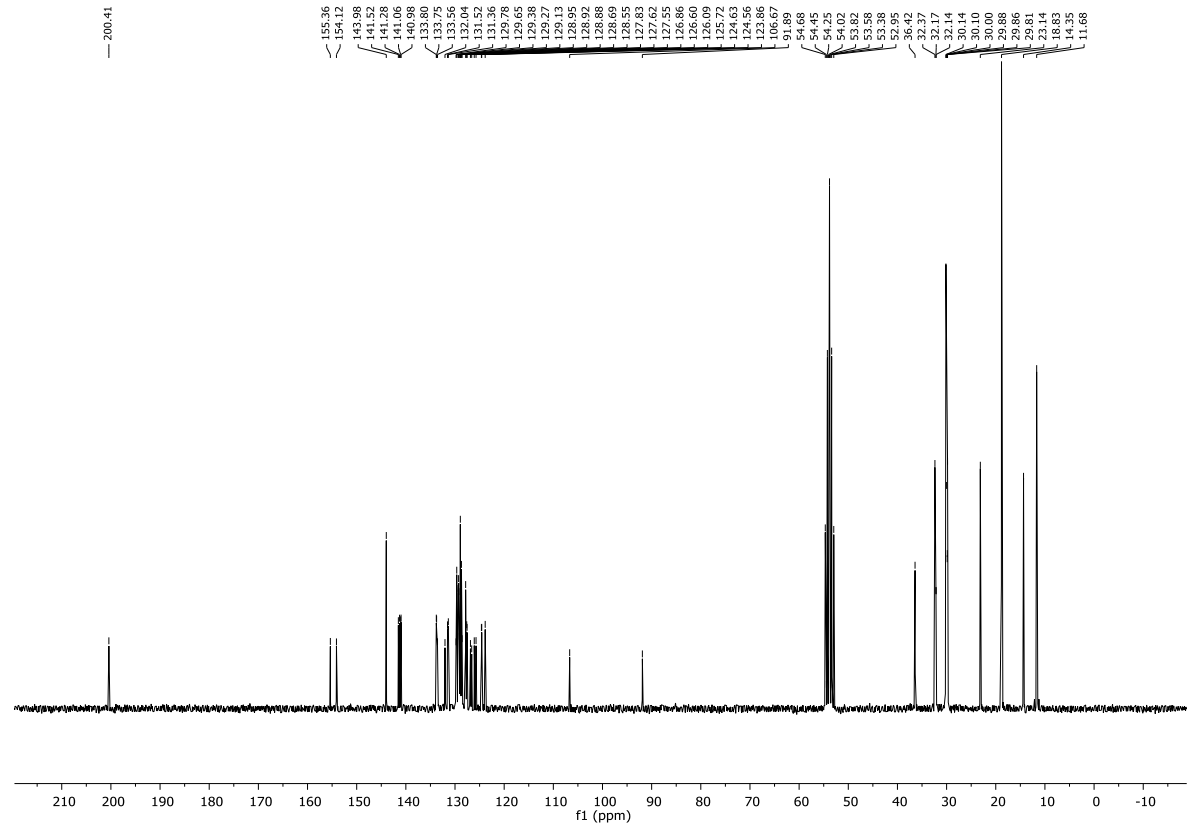

Figure S24. ^{13}C NMR spectrum of compound **S4** (62.5 MHz, CD_2Cl_2).

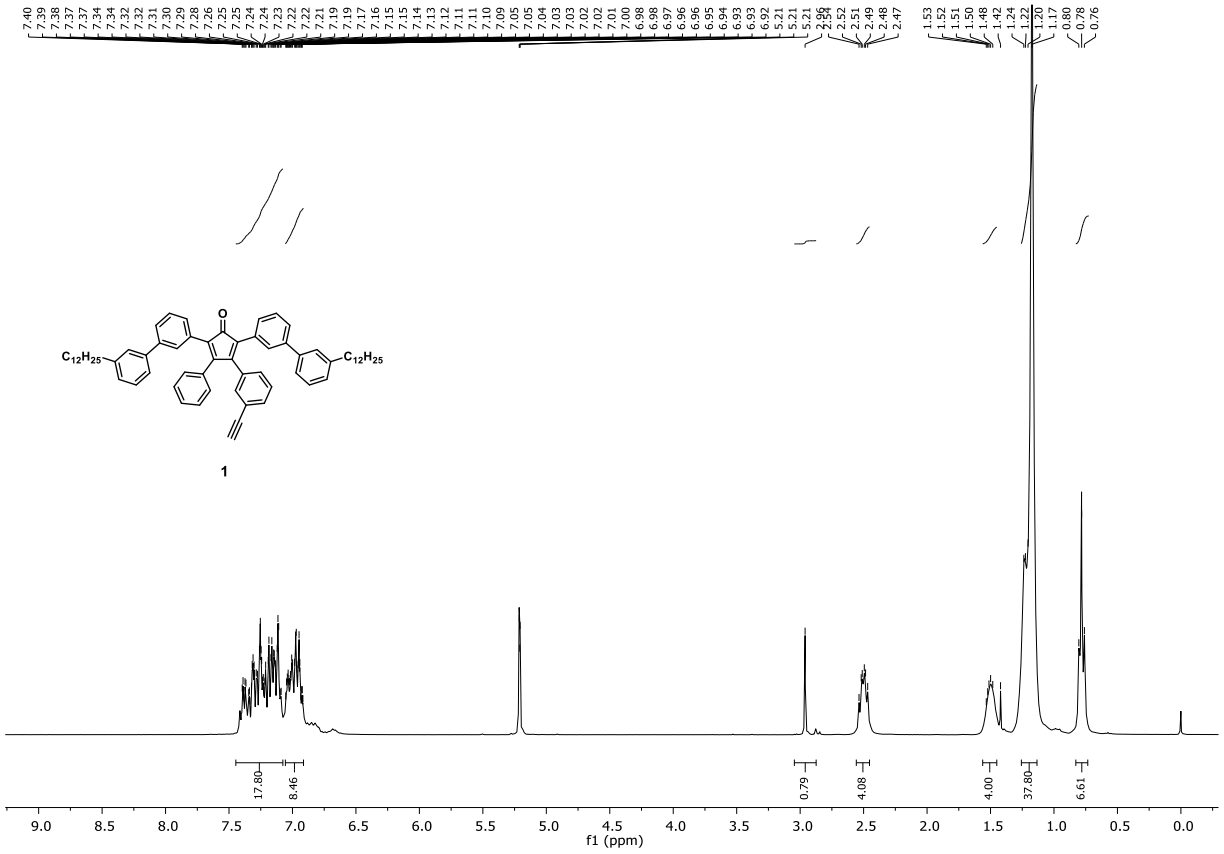

Figure S25. ^{1}H NMR spectrum of compound **1** (250 MHz, CD_2Cl_2).

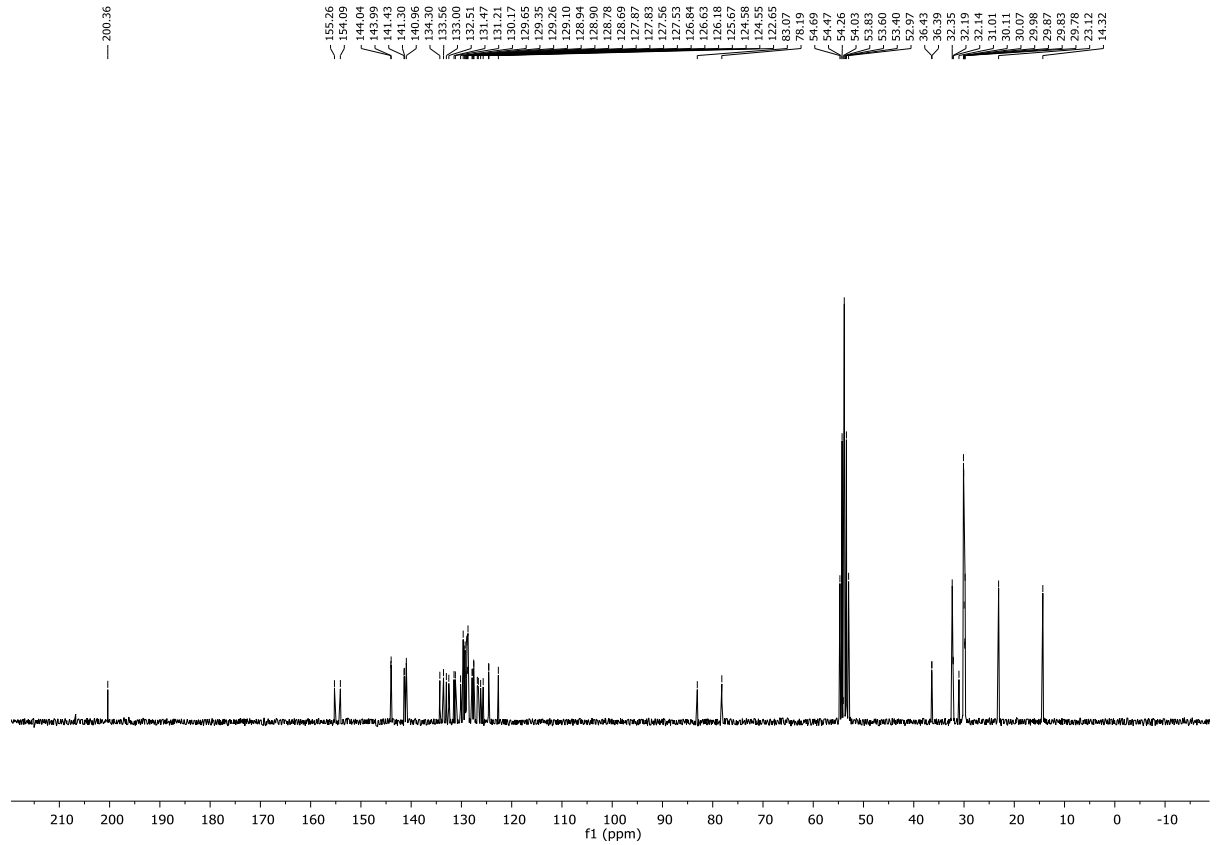

Figure S26. ^{13}C NMR spectrum of compound **1** (62.5 MHz, CD_2Cl_2).

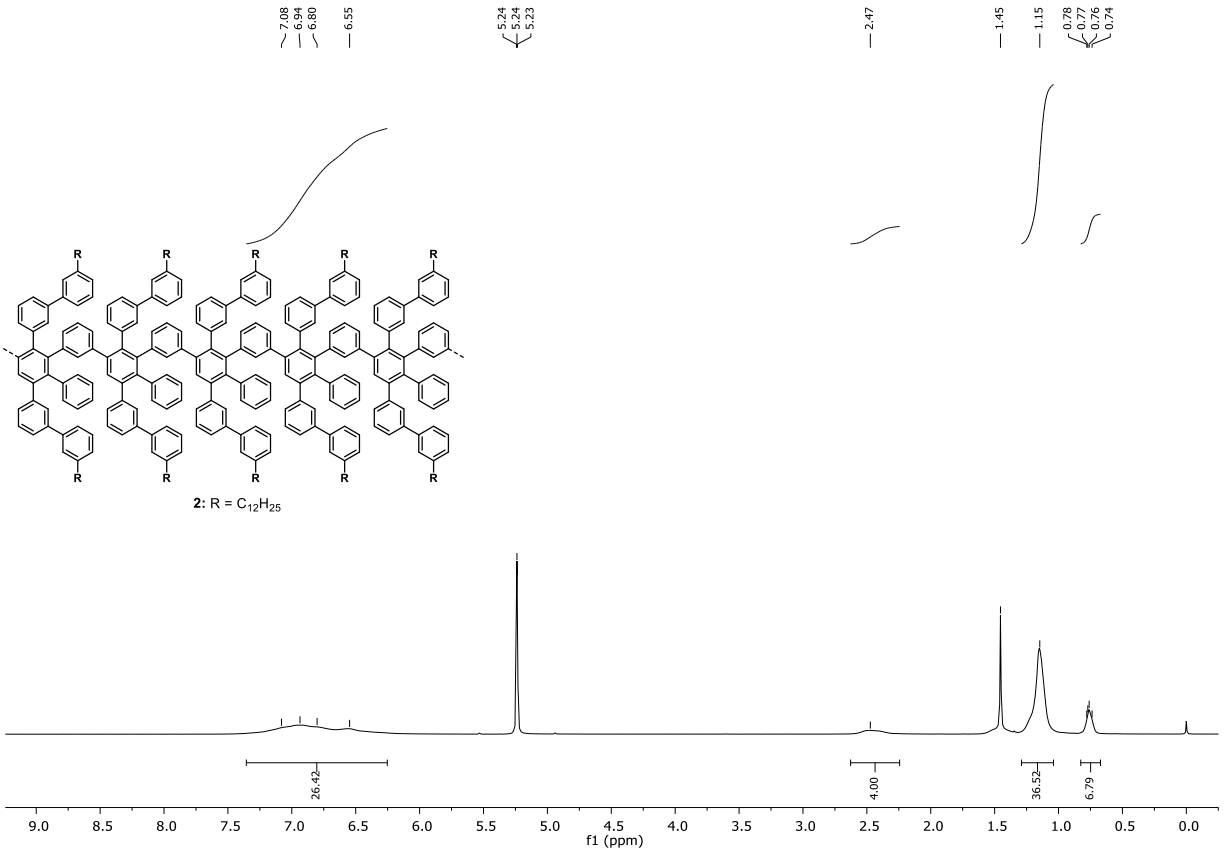

Figure S27. ^{1}H NMR spectrum of Polyphenylene precursor **2** (300 MHz, CD_2Cl_2).

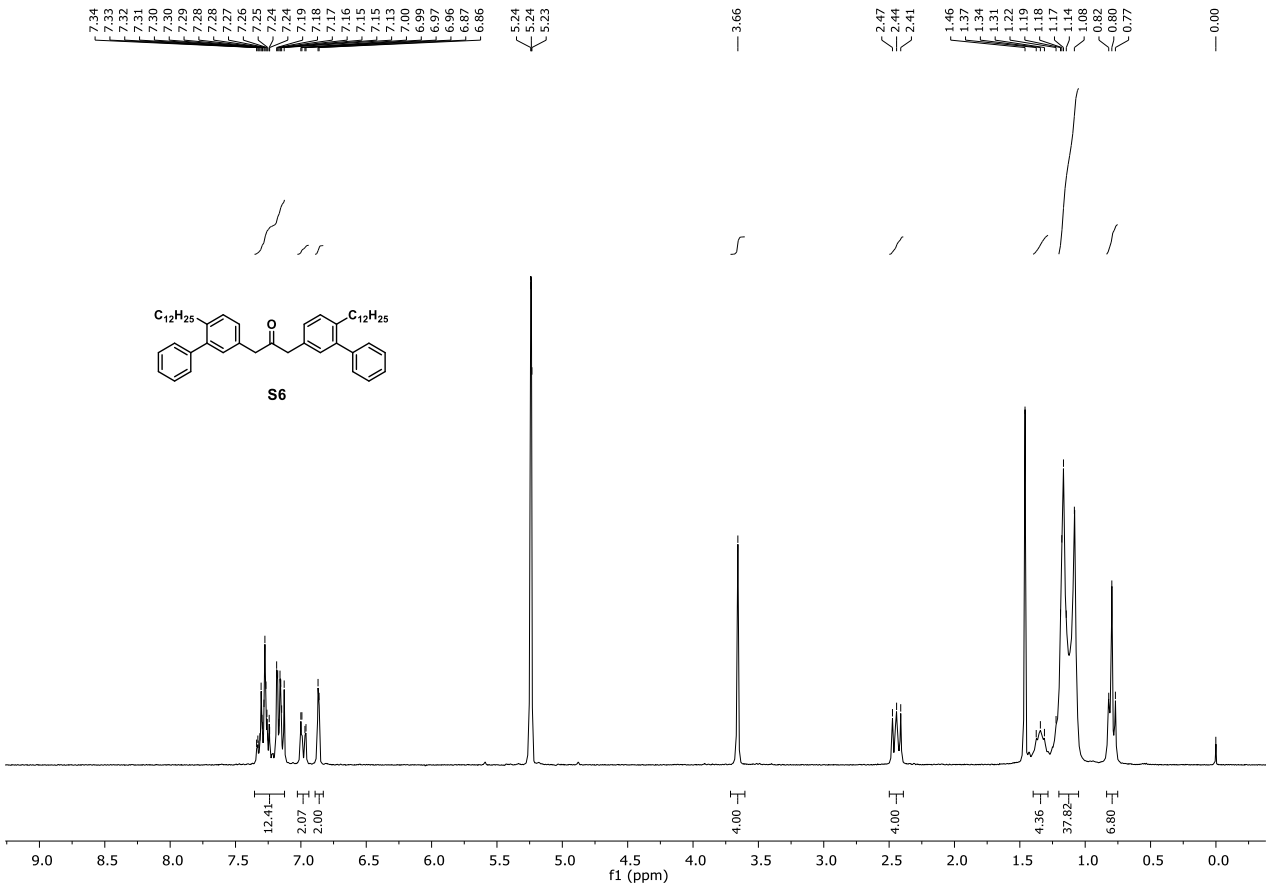

Figure S28. ^{1}H NMR spectrum of compound **S6** (250 MHz, CD_2Cl_2).

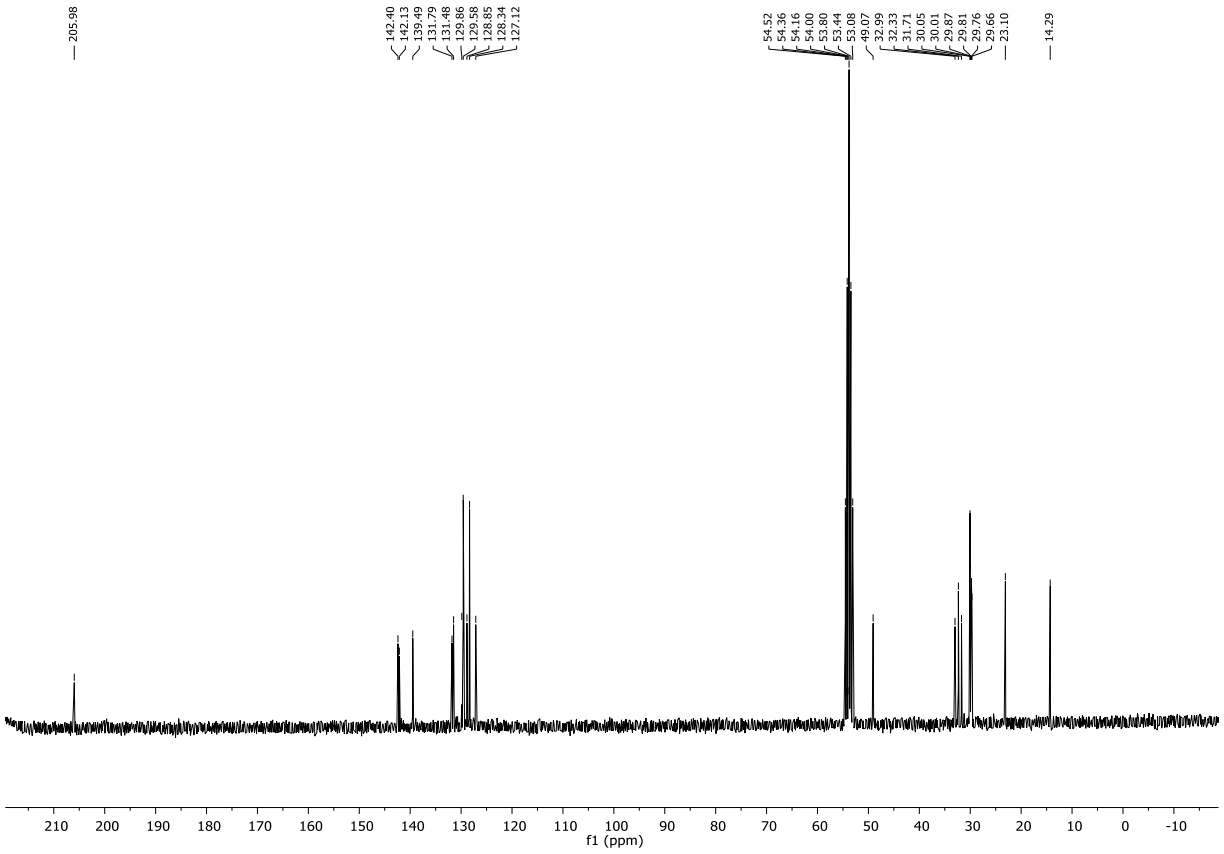

Figure S29. ^{13}C NMR spectrum of compound **S6** (75 MHz, CD_2Cl_2).

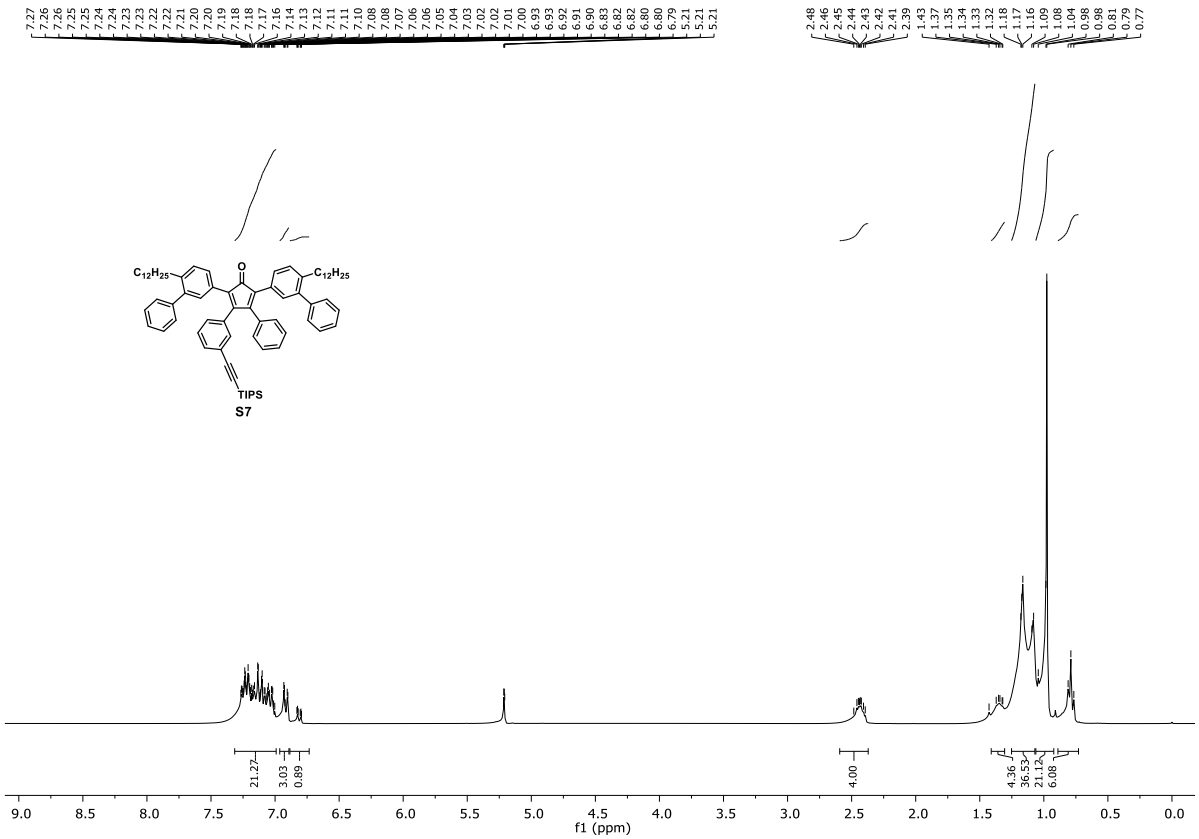

Figure S30. ^{1}H NMR spectrum of compound **S7** (300 MHz, CD_2Cl_2).

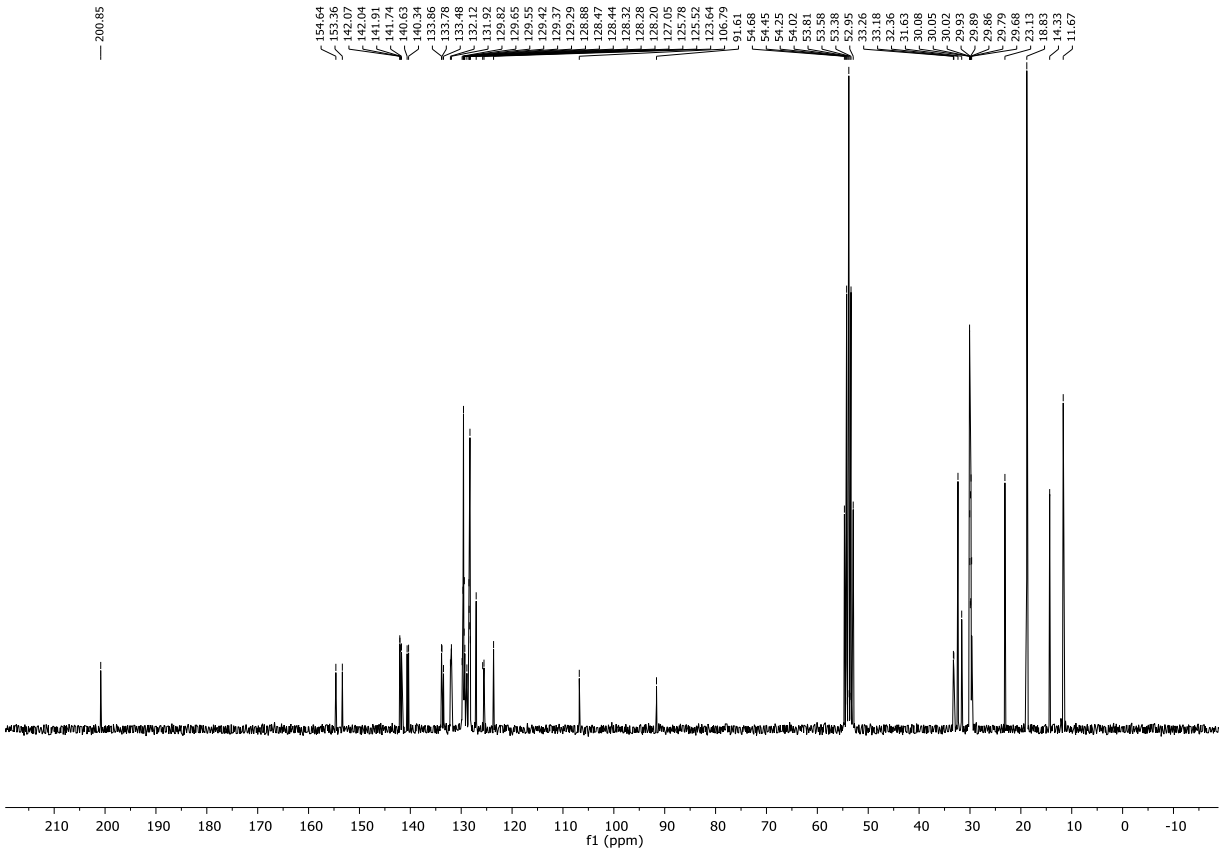

Figure S31. ^{13}C NMR spectrum of compound **S7** (62.5 MHz, CD_2Cl_2).

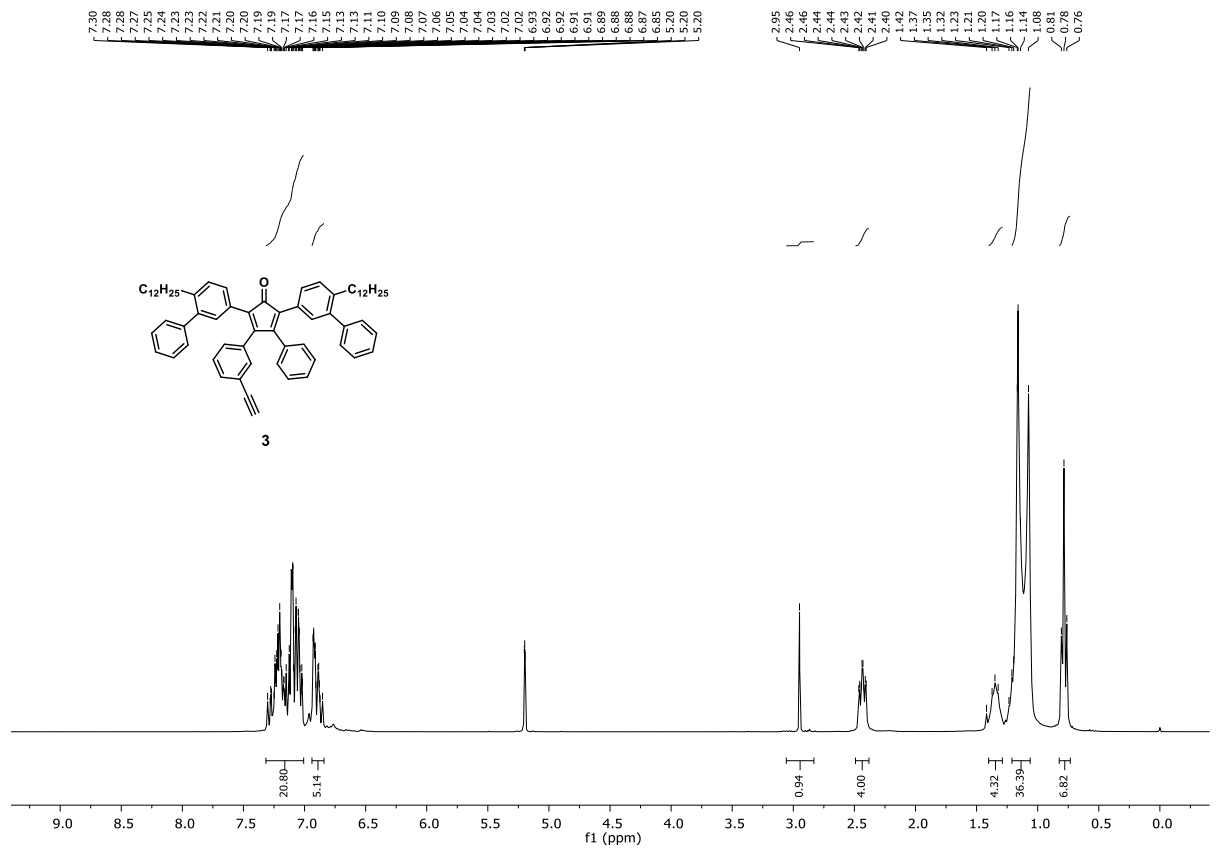

Figure S32. ^{1}H NMR spectrum of compound **3** (300 MHz, CD_2Cl_2).

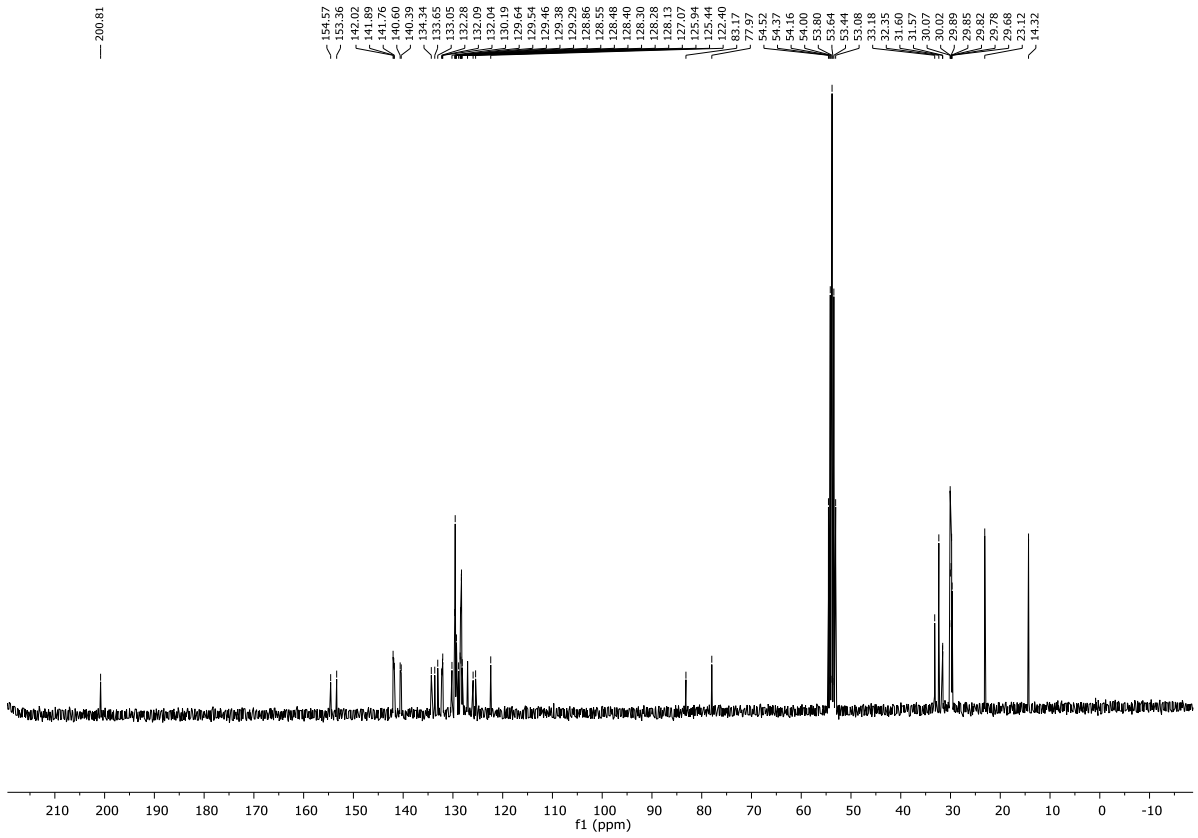

Figure S33. ^{13}C NMR spectrum of compound **3** (75 MHz, CD_2Cl_2).

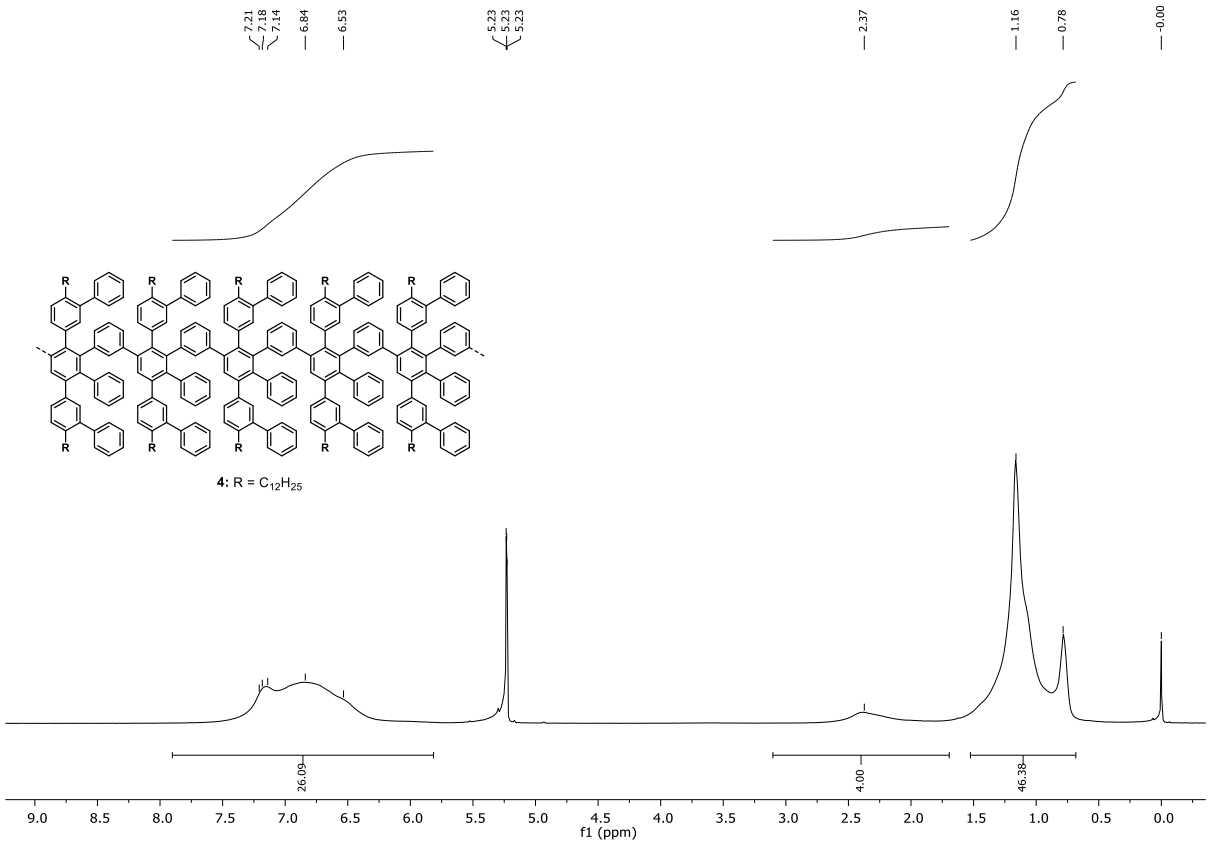

Figure S34. ^{1}H NMR spectrum of polyphenylene precursor **4** (300 MHz, CD_2Cl_2).

Reference

(1) Narita, A.; Verzhbitskiy, I. A.; Frederickx, W.; Mali, K. S.; Jensen, S. A.; Hansen, M. R.; Bonn, M.; De Feyter, S.; Casiraghi, C.; Feng, X.; Müllen, K. *Acs Nano* **2014**, *8*, 11622-11630.

(2) Tan, Y.-Z.; Yang, B.; Parvez, K.; Narita, A.; Osella, S.; Beljonne, D.; Feng, X.; Müllen, K.. *Nat. Commun.* **2013**, *4*, 2646.

(3) Chun, J.; He, L.; Byun, H. S.; Bittman, R. *J. Org. Chem.* **2000**, *65*, 7634-7640.

(4) Romer, D. R. *Synthesis-Stuttgart* **2011**, 17, 2721-2723.

(5) Baroni, S.; De Gironcoli, S.; Dal Corso, A.; Giannozzi, P. *Rev. Mod. Phys.* **2001**, *73*, 515-562.

(6) Giannozzi, P.; Baroni, S.; Bonini, N.; Calandra, M.; Car, R.; Cavazzoni, C.; Ceresoli, D.; Chiarotti, G. L.; Cococcioni, M.; Dabo, I.; Dal Corso, A.; de Gironcoli, S.; Fabris, S.; Fratesi, G.; Gebauer, R.; Gerstmann, U.; Gougoussis, C.; Kokalj, A.; Lazzeri, M.; Martin-Samos, L.; Marzari, N.; Mauri, F.; Mazzarello, R.; Paolini, S.; Pasquarello, A.; Paulatto, L.; Sbraccia, C.; Scandolo, S.; Sclauzero, G.; Seitsonen, A. P.; Smogunov, A.; Umari, P.; Wentzcovitch, R. M. *J. Phys. Condens. Matter* **2009,** *21*, 395502.

(7) Onida, G.; Reining, L.; Rubio, A. *Rev. Mod. Phys.* **2002,** *74*, 601-659.

(8) Godby, R. W.; Needs, R. J. *Phys. Rev. Lett.* **1989**, *62*, 1169-1172.

(9) Rozzi, C. A.; Varsano, D.; Marini, A.; Gross, E. K. U.; Rubio, A. *Phys. Rev. B* **2006**, *73*, 205119.

(10) Marini, A.; Hogan, C.; Grüning, M.; Varsano, D. *Comput. Phys. Commun.* **2009**, *180*, 1392-1403.

(11) Verzhbitskiy, I. A.; Corato, M. D.; Ruini, A.; Molinari, E.; Narita, A.; Hu, Y.; Schwab, M. G.; Bruna, M.; Yoon, D.; Milana, S.; Feng, X.; Müllen, K.; Ferrari, A. C.; Casiraghi, C.; Prezzi, D. *Nano Lett.* **2016**, *16*, 3442-3447.

(12) Frye, J. S.; Maciel, G. E. *J. Magn. Reson.* **1969**, 48, 125-131.

(13) Feike, M.; Demco, D. E.; Graf, R.; Gottwald, J.; Hafner, S.; Spiess, H. W. *J. Magn. Reson.* **1996**, *122*, 214-221.

(14) Saalwachter, K.; Lange, F.; Matyjaszewski, K.; Huang, C. F.; Graf, R. *J. Magn. Reson.* **2011**, *212*, 204-215.

(15) Morcombe, C. R.; Zilm, K. W. *J. Magn. Reson.* **2003**, *162*, 479-486.

(16) Shigenobu, H.; Kikuko, H. *Bull. Chem. Soc. Japan* **1991**, *64*, 685-687.

(17) Narita, A.; Feng, X. L.; Hernandez, Y.; Jensen, S. A.; Bonn, M.; Yang, H. F.; Verzhbitskiy, I. A.; Casiraghi, C.; Hansen, M. R.; Koch, A. H. R.; Fytas, G.; Ivasenko, O.; Li, B.; Mali, K. S.; Balandina, T.; Mahesh, S.; De Feyter, S.; Müllen, K. *Nat. Chem.* **2014**, *6*, 126-132.